# Empirical low-dimensional dynamics of atmospheric stable boundary layer temperature inversions

Elizabeth Ramsey and Adam H. Monahan

2022



Original citation:
Ramsey, E., & Monahan, A. H. (2022). Empirical low-dimensional dynamics of atmospheric stable boundary layer temperature inversions. *Journal of the Atmospheric Sciences*, *79*(7), 1965–1984. https://doi.org/10.1175/jas-d-21-0205.1

# Empirical Low-Dimensional Dynamics of Atmospheric Stable Boundary Layer Temperature Inversions

ELIZABETH RAMSEY[a] AND ADAM H. MONAHAN[a]

[a] *School of Earth and Ocean Sciences, University of Victoria, Victoria, British Columbia, Canada*

(Manuscript received 30 July 2021, in final form 23 March 2022)

ABSTRACT: The atmospheric stable boundary layer (SBL) is observed to display multiple regimes of stratification, flow, and turbulence. Transitions between weakly stable regimes of sustained turbulence and very stable regimes of weak turbulence are observed to occur abruptly. The understanding and predictability of turbulent recovery remains limited, reducing the accuracy of numerical weather prediction and climate projections. Idealized SBL models have related regimes to dynamically stable equilibria. Under conditions of weak energetic surface coupling, two stable branches separated by an unstable branch are predicted by these models. Such bifurcation structures are associated with rapid transitions. This work investigates the extent to which observed temperature inversion variability can be described by an empirical one-dimensional stochastic differential equation (SDE). The drift and diffusion coefficients of the SDE of observed inversion strength are approximated from statistics of their averaged time tendencies, conditioned on wind speed. Functional forms of the state dependence of these coefficients are estimated using Gaussian process regression. Probabilistic estimates of the system's deterministic equilibria are found and used to create empirical bifurcation diagrams of inversion strength as a function of wind speed. These data-driven bifurcation structures are first obtained from idealized model simulations, then repeated for observations from several meteorological towers. It is found that the effective low-dimensional dynamics of observed temperature inversions is similar to that of the idealized model. Evidence of multiple equilibria and hysteresis is found at a single site, Dome C, Antarctica, but is not robust to variations in the analysis. Evidence of state-dependent noise consistent with intermittent turbulence under very stably stratified conditions is presented.

KEYWORDS: Atmosphere; Dynamics; Boundary layer; Inversions; Stability; Climate classification/regimes; Idealized models; Single column models; Stochastic models

## 1. Introduction

Profiles of both mean states and turbulent fluxes in the atmospheric boundary layer are strongly influenced by stratification. The understanding of the stable boundary layer (SBL), usually forming at night, has lagged that of the convective boundary layer, due both to an early predominance of daytime measurements and to the smaller scale of turbulence and strong sensitivity to terrain in the SBL (Holtslag et al. 2013; LeMone et al. 2019). Detailed SBL measurements reveal a broad spectrum of different turbulent and nonturbulent structures, and unpredictable dynamics with seemingly spontaneous changes in turbulent structure (Mahrt 2014; LeMone et al. 2019; Monahan et al. 2015; Abraham and Monahan 2019b; van Hooijdonk et al. 2017a). The SBL is often classified into two regimes, the weakly stable boundary layer (wSBL) and the very stable boundary layer (vSBL) (Mahrt 1998, 2014; Holtslag et al. 2013; Monahan et al. 2015; Abraham and Monahan 2019a). The wSBL is characterized by continuous turbulence and weak stratification. Conditions classified as wSBL are associated with cloudy skies and moderate winds (Abraham and Monahan 2019a; Monahan et al. 2015). The vSBL, associated with clear skies and weak winds, is characterized by strong stratification and nearly collapsed turbulence with intermittent turbulent bursts (Abraham and Monahan 2019a; Mahrt 2014).

In general, wSBL conditions can be modeled reasonably well using classical concepts such as Monin–Obukhov similarity theory (MOST) (LeMone et al. 2019). However, in the vSBL, longwave radiative cooling from the surface strengthens temperature inversions, strongly suppressing vertical exchanges and resulting in turbulence being very localized and not well represented by MOST. As a result, the surface and the atmosphere can decouple which usually creates runaway surface cooling effect in models for weather and climate (Derbyshire 1999; Holtslag et al. 2013). Observations show intermittent turbulent bursts are one mechanism that recouple near-surface dynamical processes in the vSBL (van de Wiel et al. 2003; Mahrt 2014). Intermittent turbulent bursts are associated with processes which are often subgrid scale in operational weather and climate models such as gravity waves, low-level jets, density currents, and microfronts (Sun et al. 2002, 2004, 2015). To prevent runaway cooling in numerical weather and climate models, turbulent fluxes in the SBL are artificially increased through the use of an artificial minimum diffusivity or long-tailed similarity functions, resulting in enhanced mixing that is not justified by observations and resulting in the erosion of low-level jets, overestimation of SBL depth, and an underestimation of the wind turning height in the lower atmosphere (Holtslag et al. 2013). This simplified treatment of SBL dynamics in models decreases the accuracy of near-surface condition forecasts such as fog, frost, and air quality (Mahrt 1998, 2014). Transportation, agricultural, and renewable energy industries increasingly rely on accurate forecasts to optimize resource utilization and improve public health and safety (Holtslag et al. 2013; Sommerfeld et al. 2019).

*Corresponding author*: Elizabeth Ramsey, monahana@uvic.ca

DOI: 10.1175/JAS-D-21-0205.1

No single variable has been found to predict SBL regime transitions (Abraham and Monahan 2019b; Monahan et al. 2015). Transitions between regimes, both from wSBL to vSBL (turbulent collapse) and from vSBL to wSBL (turbulent recovery) are frequent and both types of regime transition can occur within a single night (Abraham and Monahan 2019b). Some nights are observed to occupy a single regime whereas other nights experience multiple regime transitions (Abraham and Monahan 2019b). Transitions occur abruptly and have not been reliably predicted (Abraham and Monahan 2019c; Kaiser et al. 2020; van Hooijdonk et al. 2017a). In a dynamical systems context, unpredictable transitions are often found to be associated with bifurcations.

The concept of a maximum sustainable heat flux (MSHF) was introduced in van de Wiel et al. (2012a,b), offering a new conceptual framework for modeling SBL regime occupation. This framework builds on results from an idealized single column SBL model with fixed surface energy flux (van de Wiel et al. 2007). For this model, it was shown that turbulence can be maintained if turbulent heat fluxes balance net radiative surface cooling for a given wind shear. Otherwise, turbulence collapses, surface temperature decreases and stability increases, creating vSBL conditions. A critical wind speed at which turbulence collapses can then be derived. Using meteorological tower observations from Cabauw, van Hooijdonk et al. (2015) and Monahan et al. (2015) showed that regimes can be reasonably separated using MSHF.

The assumption of a fixed surface heat flux was relaxed in van de Wiel et al. (2017, hereafter vdW17) by coupling the atmospheric and surface energy budgets in an idealized model. The model fixes wind speed at a reference height allowing wind speed to be a constant external parameter to the system. Energetic coupling between the atmosphere and the surface is controlled by a single parameter, $\lambda$. The equilibrium solutions to this conceptual model for various model parameters are considered in vdW17. The vSBL is associated with a dynamically stable equilibrium branch with strong temperature inversions at relatively low wind speeds. The wSBL is associated with a dynamically stable equilibrium branch with weak temperature inversions at larger wind speeds. For large values of $\lambda$ (relatively strong energetic coupling), vSBL and wSBL states are connected by a dynamically stable transitional equilibrium branch. For low values of $\lambda$ (such as over a thermally insulating surface such as snow), the stable equilibrium temperature inversion values differ substantially and are separated by a dynamically unstable equilibrium branch. For these values of $\lambda$, both stable branches coexist with the unstable branch over a range of wind speeds. Similar dependencies of the equilibrium structure on model parameters are observed for changes in isothermal net radiation and surface roughness. Suggestive evidence of such multiple equilibria and hysteresis was provided in scatterplots of observations from Dome C, Antarctica, in vdW17 and Vignon et al. (2017b). The existence of multiple equilibria and bifurcations could explain the abrupt regime transitions observed. In this dynamical systems context, transitions are initiated by changes in external forcing or by perturbations from processes not accounted for in this idealized model.

Kaiser et al. (2020) empirically investigated the predictions of vdW17 using high-resolution temperature time series data. The approach described in Faranda et al. (2014) was considered, in which early warning indicators of regime transitions are diagnosed as changes in the parameters of an autoregressive moving average model (ARMA) fit to moving windows of the time series data. This method allows for a statistical quantification of the dynamical stability of observables, such that increases on the order of the ARMA models are taken to represent a reduction of dynamical stability. This methodology is a generalization of the early warning system indicator method proposed in Scheffer et al. (2009), where bifurcations are detected as increases in autocorrelation times as the system approaches a critical transition. Kaiser et al. (2020) first tested the approach using a model inspired by but different than the vdW17 model. An additive white noise term was added to the model to represent small fluctuations in temperature inversions due to processes not accounted for in the highly simplified model. Using data from meteorological towers in Dumosa, Australia, and Dome C, Antarctica, they determined that a sampling frequency of at least 1 min is required to reliably predict regime transitions using this methodology. The results from the Dumosa tower suggest the existence of one dynamically stable branch and one dynamically unstable branch, while the Dome C tower was found to have insufficient time resolution to detect unstable branches.

The present study investigates the extent to which an entirely data-driven approach can be used to represent the observed variability of temperature inversions as a low-dimensional dynamical system such as that proposed in vdW17, using a methodology that is distinct from that of Kaiser et al. (2020). Empirical demonstration of such effective low-dimensional structure provides evidence that the vdW17 model captures essential features of the physical controls on SBL structure. We adopt a semiparametric approach based on Siegert et al. (1998) in which deterministic and stochastic components of a one-dimensional stochastic differential equation (SDE) are estimated from time series of inversion strength, conditioned on wind speed. We use Gaussian process regression (GPR) to fit functional forms to the state dependence of the drift and diffusion functions of the empirical SDE. Deterministic equilibria at each wind speed bin are then computed from the GPR fits to drift coefficients. This analysis results in empirical bifurcation curves of equilibrium temperature inversions as functions of wind speed. The use of GPR fits allows for uncertainty quantification of the estimated equilibria. The empirically derived diffusion coefficients provide insights into the potential state dependence of stochastic terms appropriate for this simplified one-dimensional representation of the SBL. Similar to Kaiser et al. (2020), the methodology is first tested using realizations from a stochastic generalization of the vdW17 model. We then apply the analysis to observed temperature inversion time series from a number of meteorological towers around the world, in a range of meteorological settings.

The vdW17 model is introduced and nondimensionalized in section 2, followed by a description of the method used to estimate stochastic dynamics from time series data. In section 3,

the stochastic vdW17 model is used to assess this methodology and its sensitivity to how the observations are processed. Observationally based equilibrium structures and diffusion coefficients are obtained in section 4. A discussion and conclusions are presented in section 5.

## 2. Methods

### a. *The van de Wiel et al. (2017) model*

This section describes the vdW17 model, introduces the nondimensional form of the model, and describes its stochastic extension considered to test our method. A key limitation of the original MSHF framework introduced in van de Wiel et al. (2012a,b) is that it cannot predict SBL behavior when wind speeds fall below a critical wind speed value. It was hypothesized that the lack of such an equilibrium state results from the fixed surface heat flux, and that feedback mechanisms such as soil heat transport and surface cooling prevent runaway longwave radiative cooling and allow for a new thermodynamic equilibrium to be reached. This equilibrium state would correspond to the vSBL regime, whereas the equilibrium found at larger wind speeds would correspond to the wSBL regime. These feedbacks are included in the vdW17 model. The vdW17 model models the near-surface temperature inversion in terms of a highly idealized surface energy budget. The model begins with the notion of the velocity crossing point introduced in van de Wiel et al. (2012a,b), defined as a reference height $z_h$ at which the wind speed $U$ is approximately steady during the duration of stable stratification. The assumption of the existence of such a height allows $U$ to be taken as an external parameter to the system. The temperature inversion is measured as the temperature difference between $z_h$ and the surface, $\Delta T = T_h - T_s$. A linear relationship between ground heat flux density and inversion strength is assumed using the surface conductance parameter $\lambda_s$: $G = \lambda_s \Delta T$. The net longwave radiation flux density $Q_n$ is modeled as the sum of a constant isothermal radiative flux density $Q_i$ and a linear Planck feedback term $\lambda_{\mathrm{lw}}\Delta T$. The surface turbulent sensible heat flux is modeled using a stability function $f(R_b)$, where $R_b$ is the bulk Richardson number, $R_b = z_h(g/T_h)(\Delta T/U^2)$. The resulting, parameterized equation for the model is

$$C_v \frac{d\Delta T}{dt} = Q_i - \lambda \Delta T - \rho c_p c_D U \Delta T f(R_b), \tag{1}$$

where $C_v$ (J m$^2$ K$^{-1}$) is the heat capacity of the surface, $\lambda = \lambda_s + \lambda_{\mathrm{lw}}$ (J m$^{-2}$ s$^{-1}$ K$^{-1}$) is lumped parameter controlling the energetic coupling between the atmosphere and the surface, $\rho$ (kg m$^{-3}$) and $c_p$ (J kg$^{-1}$ K$^{-1}$) are the air density and specific heat capacity at a constant pressure, $c_D = [\kappa/\ln(z_h/z_0)]^2$ is the neutral drag coefficient with $\kappa \approx 0.4$, and $z_0$ is the roughness length. In our analysis we use a Businger–Dyer-type stability function:

$$f(R_b) = \begin{cases} 1 - \alpha R_b & R_b \le 1/\alpha, \\ 0 & R_b > \alpha, \end{cases} \tag{2}$$

with $\alpha = 5$. All variables in Eq. (1) should be interpreted as Reynolds-averaged quantities.

TABLE 1. Nondimensional model parameters.

| Parameter | Description | Value |
|---|---|---|
| $\hat{Q}$ | Isothermal net radiation | $3 \times 10^{-6}$ to $3 \times 10^{-5}$ |
| $\hat{\lambda}$ | Surface exchange coefficient | $8 \times 10^{-5}$ to $4 \times 10^{-4}$ |
| $c_D$ | Neutral drag coefficient | $1.3 \times 10^{-3}$ |
| $\eta$ | Additive noise intensity | $6 \times 10^{-5}$ to $1.5 \times 10^{-3}$ |
| $\overline{U}$ | Mean wind speed | 1 |
| $\eta_U$ | Wind speed variance | 0.7 |
| $\widehat{\tau_U}$ | Wind fluctuation time scale | $1 \times 10^3$ to $3 \times 10^6$ |
| $N$ | Number of data points subsampled | $10^4$ to $10^6$ |
| $\Delta t$ | Time step | 30 |
| $n_t$ | Sampling rate | 10 |

In this study a nondimensionalized form of the vdW17 model is considered. The dimensional scales of the model are defined as

$$\begin{aligned} T_{\mathrm{sc}} &= T_r && \text{(temperature)}, \\ L_{\mathrm{sc}} &= \frac{C_v}{\rho c_p} && \text{(length)}, \\ \upsilon_{\mathrm{sc}} &= (g z_r)^{1/2} && \text{(speed)}, \\ t_{\mathrm{sc}} &= \frac{C_v}{\rho c_p (g z_h)^{1/2}} && \text{(time)}. \end{aligned} \tag{3}$$

The nondimensional form of Eq. (1) becomes

$$\frac{dx}{ds} = \hat{Q} - \hat{\lambda} x - c_D \hat{U} f\left(\frac{x}{\hat{U}^2}\right) x \tag{4}$$

with nondimensional time, $s = t/t_{\mathrm{sc}}$, and the nondimensional state variable, $x = \Delta T/T_{\mathrm{sc}}$. Carets denote nondimensionalized parameters, summarized in Table 1. Note that the dimensional scales used in this study differ from those in vdW17 and Kaiser et al. (2020) which uses $U$ to define the dimensional scales. Our alternative nondimensionalization allows us to accommodate the nonlinear dependence of the stability function on wind speed, and to allow for all of $\hat{Q}$, $\hat{\lambda}$, and $\hat{U}$ to be retained as bifurcation parameters. For the latter reason none of $Q$, $\lambda$, or $U$ are used in defining the dimensional scales. The nondimensionalization of the vdW17 model in Kaiser et al. (2020) makes it difficult to separate the effects of wind speed and surface roughness and impossible to explicitly model variable wind speed, as we do in section 3. The sensitivity of the model to values of $\hat{Q}$ and $\hat{\lambda}$ is explored in section 3.

It is possible that small-scale perturbations to the SBL may be related to transitions from the vSBL to the wSBL, since no single state variable has been found to predict these transitions (Mahrt 2014; Monahan et al. 2015; Abraham et al. 2019; Kaiser et al. 2020). Observations of the SBL show intermittent, stochastic turbulent bursts, particularly in the vSBL, which are not explicitly accounted for in the vdW17 model (van de Wiel et al. 2003; Mahrt 2014). Many other processes are also not represented in the simplified form of the vdW17 model, including nonturbulent submesoscale motions. These facts motivate the addition of a stochastic term to the vdW17

model to represent subgrid-scale processes in the SBL. A general SDE small-scale, unrepresented processes, resulting in the vdW17 model taking the form of an SDE for the $d$-dimensional stochastic process $\mathbf{X}(t)$ is given by

$$\frac{d}{dt}\mathbf{X}(t) = \mathbf{f}(\mathbf{X}(t), t) + \mathbf{g}(\mathbf{X}(t), t)\dot{\mathbf{w}}, \tag{5}$$

where $\mathbf{X}(t)$ is a time-dependent $d$-dimensional stochastic process, $\mathbf{f}(\mathbf{X}(t), t)$ is the deterministic part of the tendency known as the drift, and $\dot{\mathbf{w}}$ represents a vector of $r$ mutually independent Gaussian white noise processes (Gardiner 1990; Penland 2003). The $d \times r$ diffusion matrix $\mathbf{g}(\mathbf{X}(t), t)$ defines the stochastic part of the tendency. In the context of the vdW17 model, the diffusion matrix represents any processes not explicitly defined in the deterministic part of the equation, such as intermittent turbulent flux, gravity waves and katabatic flows. If the diffusion coefficient is a function of time only, $\mathbf{g}(t)$, then $\mathbf{X}(t)$ is said to be an additive noise process. The diffusion coefficient can also be a function of the state of the system $\mathbf{g}(\mathbf{X}(t), t)$ defining multiplicative noise.

When the noise is multiplicative, it is necessary to distinguish between different forms of stochastic calculus (Gardiner 1990; Penland 2003). Solutions to SDEs are defined in terms of integrals over white noise processes. Because of the delta function autocorrelation structure of the noise, the value of the integral depends on how the Riemann sum is defined. Equation (5) is expressed in Itô form, as is natural for the estimation procedure from discrete data for the drift and diffusion described below. The Stratonovich form is the natural definition of the SDE when the white noise process is an approximation to driving processes with finite autocorrelation. The Stratonovich form of the SDE would be more appropriate in this context, as according to the Wong–Zakai theorem real world systems approximated by white noise converge to the Stratonovich form of the SDE (Twardowska 1996). While it is possible in principle to convert the diffusion coefficient to the other standard form, the Stratonovich, this requires computation of the derivative of the diffusion coefficient, which is problematic if the data are noisy. In the limit of additive noise, the two SDEs are identical (Gardiner 1990; Penland 2003). We discuss the implications of analyzing the SDEs represented in Itô form in section 5. The white noise representation for processes not included in vdW17 is a good approximation if the time scales of the unresolved processes are short relative to the dynamical time scale (Monahan and Culina 2011). While this time scale separation is not likely to exist, we retain it for mathematical convenience.

In our analysis of vdW17 simulations in section 3, we consider additive white noise, similar to the model used in Kaiser et al. (2020). The form of the additive stochastic vdW17 model in nondimensional form [Eq. (4)] is

$$\frac{dx}{ds} = \hat{Q} - \hat{\lambda}x - c_D\hat{U}f\left(\frac{x}{\hat{U}^2}\right)x + \eta\dot{w}, \tag{6}$$

where $\eta$ is the diffusion coefficient of the model. Note that the use of the word "diffusion" in the context of the noise term follows from the early use of SDEs to model Brownian motion; the associated term is not associated with diffusive processes in the SBL (although it is related to turbulent ones).

Consideration of the stochastic extension of the vdW17 model allows us to assess the accuracy and robustness of the empirical reconstruction procedure we also use on data from tower observations. Use of an additive noise generalization provides a benchmark for how apparent multiplicative noise structure can emerge from estimation biases or the effects of data processing. We use this benchmark in our interpretation of the reconstructed dynamics from tower observations.

### b. *Empirical reconstruction procedure*

#### 1) Data-driven stochastic parameterization

As discussed in vdW17 and Holdsworth and Monahan (2019), $\Delta T$ modeled by the vdW17 model [Eq. (1)] is highly dependent on parameters that are difficult to accurately quantify, such as the $C_v$, the $\lambda_s$, and $z_0$. The model also parameterizes the effect of atmospheric stability on turbulent heat transport using the semi-empirical function $f(R_b)$ for which several forms have been proposed (Holdsworth et al. 2016; vdW17). The functional form of this highly idealized near-surface atmospheric energy model is therefore uncertain. Rather than try to directly fit this model to observations, we investigate the effective low-dimensional dynamics of $\Delta T$ using an entirely data-driven approach. We assume only that the tendency of $\Delta T$ is a function of $\Delta T$ and $U(z_h)$. Estimating equilibrium curves using a data-driven approach will provide empirical insights into the extent to which the SBL displays effective low-dimensional dynamics similar to those of the vdW17 model. The nature of noise related to "unresolved processes" represented in the diffusion term also remains uncertain, as explored in Abraham et al. (2019). Deriving a diffusion term from data will help guide future conceptualizations of such processes in this system.

In particular, we use the method of estimating the stochastic dynamics producing time series data, without assuming functional forms for the drift and diffusion, presented by Siegert et al. (1998) and Friedrich et al. (2000). If the drift and diffusion terms of Eq. (5) do not explicitly depend on time and noise is white, knowing the state of the system at one time in the past is sufficient to represent the statistical behavior of future states, defining a stationary Markovian system. Therefore, the statistics of the state variable $\mathbf{X}$ evolving from a state $\mathbf{X}(t)$ to a state $\mathbf{X}(t + \tau)$ can be used to empirically determine the drift and diffusion coefficients. It can be shown that in the limit of $\tau \to 0$ the drift coefficient is given by the conditional mean of the time tendency of the system,

$$\mathbf{f}(\mathbf{X}) = \lim_{\tau\to 0}\frac{1}{\tau}\langle \mathbf{X}(t+\tau) - \mathbf{X}\rangle\Big|_{\mathbf{X}(t)=\mathbf{X}} \tag{7}$$

and the diffusion matrix can be recovered from the limiting conditional covariance,

$$\mathbf{g}(\mathbf{X})\mathbf{g}^{\mathrm{T}}(\mathbf{X}) = \lim_{\tau\to 0}\frac{1}{\tau}\langle [\mathbf{X}(t+\tau) - \mathbf{X}][\mathbf{X}(t+\tau) - \mathbf{X}]^T\rangle\Big|_{\mathbf{X}(t)=\mathbf{X}}, \tag{8}$$

where $\langle\cdot\rangle$ denotes the expectation operator (Gardiner 1990). The reconstructed SDE is interpreted in the Itô sense.

In practice, the $\tau \to 0$ limit cannot be taken using discrete time series data. The need to use a finite data sampling interval $\Delta t$ is a known limitation of this methodology (Friedrich et al. 2011). Sura and Barsugli (2002) discuss numerical errors in drift and diffusion coefficients due to finite sampling rates by expanding the Itô Taylor series $\mathbf{X}(t + \Delta t)$ to leading order $\Delta t^2$. They show that finite differencing creates errors in $\mathbf{f}$ and $\mathbf{g}$ that are nonlinear and coupled with, to a leading order, a quadratic bias in $\mathbf{g}$. This bias will be investigated using numerical simulations of the stochastic vdW17 model in section 3. The consequences of working with a nonautonomous system because of explicit time dependence of the wind speed are investigated using the vdW17 model in section 3.

### 2) GAUSSIAN PROCESS REGRESSION

The finite difference approximation to Eqs. (7) and (8) estimates drift and diffusion values at discrete points; however, a continuous function is desired. To determine functional forms for the deterministic part of the model $\mathbf{f}(\mathbf{X})$ and the stochastic part of the model $\mathbf{g}(\mathbf{X})$, we use the probabilistic machine learning method GPR (e.g., Rasmussen and Williams 2006). Gaussian processes (GP) are an extension of multivariate Gaussian probability distributions to the space of functions. A GP is an infinite collection of random variables, any finite number of which have a Gaussian distribution. From a statistical perspective, GPs can be thought of as defining a probability distribution over all possible functions that fit a set of points. The probabilistic nature of GPR allows for a natural quantification of the uncertainty of statistical fits. The use of GPR obviates the need to estimate discrete approximations to the drift and diffusion by binning the observations $\mathbf{X}$ (e.g., García et al. 2017).

GPs are completely specified by their mean $m(\mathbf{X})$ and covariance $K(\mathbf{X}, \mathbf{X}')$ functions, giving a GP $\phi(\mathbf{X}) \sim \mathcal{GP}(m(\mathbf{X}), K(\mathbf{X}, \mathbf{X}'))$. The squared exponential kernel defined as

$$K(\mathbf{X}_i, \mathbf{X}_j) = \sigma_f^2 \exp\left[-\frac{(\mathbf{X}_i - \mathbf{X}_j)^2}{2l^2}\right] + \sigma_n^2 \delta_{i,j} \tag{9}$$

is infinitely differentiable and therefore produces smooth realizations. For this reason it is commonly used and a suitable choice for this application (Rasmussen and Williams 2006). Estimation of the GP $\phi(\mathbf{X})$ conditioned on discrete observations $\phi(\mathbf{X}_o)$ is implemented in a Bayesian framework. Prior expectations of form of the mean of the GP can be defined using an explicit basis function, as discussed in more detail in the next subsection. Maximum likelihood estimates of GPR parameters $\sigma_f$, $\sigma_n$, and $l$ are found numerically. A detailed development of the posterior distribution of the GP conditioned on the observations $\phi(\mathbf{X_o})$ is presented in Rasmussen and Williams (2006).

Knowing the mean and covariance, a realization from a GPR model at the points $\mathbf{X}_*$ can be generated as

$$\phi(\mathbf{X}_*) = m(\mathbf{X}_*) + \mathbf{L}\mu, \tag{10}$$

where $\mathbf{L}$ is the Cholesky decomposition of the positive-definite covariance matrix, $K(\mathbf{X}_*, \mathbf{X}_*)$ is a way of defining the square root of a matrix, and $\mu$ is a mean-zero, unit-variance Gaussian distributed random variable of the same dimensions as $\mathbf{X}_*$. By generating realizations of the drift function from the GP fit to observations, we can quantify the uncertainty in the number and positions of equilibria of the deterministic dynamics.

### 3) THE ESTIMATION METHOD

Previous sections described the theoretical framework used to empirically investigate the extent to which tower observations of the SBL follow the framework described by the vdW17 method. This section describes how these methods are combined for this empirical investigation, and for sensitivity tests of method performed using vdW17 model output. While we do not fit observations to the vdW17 model, the empirical reconstruction procedure is motivated by similar assumptions to this model. For each observational dataset we consider, we first define the velocity crossing point $z_h$ as the measurement altitude with the longest autocorrelation time scale over the course of a night (indicated in Table 2). The temperature inversion $\Delta T$ is defined based on the temperature difference between $z_h$ and the lowest observational level (which differs across the different datasets). Discrete observed values of $\Delta T$ that are less than $-z_h\Gamma_d$ (where $\Gamma_d$ is the dry adiabatic lapse rate) are removed from the analysis as statically unstable points are not of interest. Similarly, values of $x$ modeled in the nondimensionalized stochastic vdW17 that are less than zero are removed from the analysis. Observed values of $\Delta T$ (or idealized model values of $x$) are conditioned on $U(z_h)$ [for observations of $U(z_h)$], using $N_U$ bins across the range of $N$ observed $U$ values. The value of $N_U$ is chosen to be large enough that $U$ does not vary substantially within a bin, while still being small enough for each $U$ bin to be well populated. Bins with more than 1000 points are split into two to provide finer wind resolution when data are sufficient. We found from empirical investigation that $N_U = 30$ to $N_U = 50$ were most appropriate for the dataset sizes considered in this study. A wide range of $U$ sizes were tested and in general results did not qualitatively differ.

Within each $U$ bin, the drift and diffusion coefficient are estimated from the time tendencies of data [Eqs. (7) and (8)]. To obtain continuous drift and diffusion functions, two separate GP models are defined, one for the conditional drift coefficient $\hat{f}_U \sim \mathcal{GP}(m_f(\Delta T), K_f(\Delta T, \Delta T'))$, and one for the conditional diffusion coefficient $\hat{g}_U \sim \mathcal{GP}(m_g(\Delta T), K_g(\Delta T, \Delta T'))$. The resulting empirically derived single column SBL model can be expressed as

$$\frac{\Delta T_U}{\Delta t} = \hat{f}_U(\Delta T_U) + \hat{g}_U(\Delta T_U)\dot{w} \tag{11}$$

for each binned $U$, giving a set of $N_U$ empirical SDE's, each of which are estimated separately. Note that subscripts $U$ have been added to Eq. (11) to highlight that equations are conditioned on wind speed. A visualization of this approach is shown in Fig. 1.

TABLE 2. Summary of meteorological weather tower data used, sorted alphabetically. Detailed information about each site can be found in the cited references. This table is adapted from Abraham and Monahan (2019a). Information on data availability can be found in the acknowledgments.

| Institute | References | Location | Time period | Points | Data | Avg (min) | Measurement heights (m) | $z_h$ (m) |
|---|---|---|---|---|---|---|---|---|
| Royal Netherlands Meteorological Institute (KNMI), Cabauw, Netherlands | Van Ulden and Wieringa (1996), Bosveld et al. (2020) | 51.9700°N, 4.9262°E, −0.7m | 2001–19 | $5.6 \times 10^5$ | $T$<br>$U$<br>$Q$ | 10<br>10<br>10 | 2, 10, 20,50, 80, 140, 200<br>10, 20, 40, 80, 140, 200<br>1.5 | 40 |
| Meteorologisches Institut der Universität Hamburg (MI), Hamburg, Germany | Brümmer et al. (2012), Gryning et al. (2016) | 53.5192°N, 10.1051°E, 0.3m | 2005–15 | $2.74 \times 10^6$ | $T$<br>$U$ | 1<br>1 | 2, 10, 50, 110, 175, 250, 280<br>10, 50, 110, 175, 250, 280 | 50 |
| Karlsruhe Institut fur Technologie (KIT), Karlsruhe, Germany | Barthlott et al. (2003), Kohler et al. (2018), Wenzel et al. (1997), Kalthoff and Vogel (1992) | 49.0925°N, 8.4258°E, 110.4m | 2003–13 | $1.3 \times 10^5$ | $T$<br>$U$ | 10<br>10 | 2, 10, 30, 60, 100, 130, 160, 200<br>2, 20, 30, 40, 50, 60, 80, 100, 130, 160, 200 | 60 |
| Los Alamos National Laboratory (LANL), Los Alamos, United States | Bowen et al. (2000), Bruggeman (2017) | 35.8614°N, 106.3196°W, 2263m | 1995–2015 | $2.7 \times 10^5$ | $T$<br>$U$<br>$Q$ | 15<br>15<br>15 | 1.2, 11.5, 23, 46, 92<br>11.5, 23, 46, 92<br>1.5 | 46 |
| Institut Polaire Français Paul Émile Victor (IPEV), and Programma Nazionale Ricerche in Antartide (PNRA), Dome C, Antarctica | Genthon et al. (2021), Vignon et al. (2017b), Vignon et al. (2017a), Genthon et al. (2010), Genthon et al. (2013) | 75.1000°S, 123.3000°E, 3233m | 2011–18 | $9 \times 10^4$ | $T$<br>$U$<br>$Q$ | 30<br>30<br>30 | 1.3, 2.3, 3.5, 9.0, 18.2, 25.6, 32.9, 41.3<br>1.3, 2.3, 3.5, 9.0, 18.2, 25.6, 32.9, 41.3<br>1.5 | 9 |

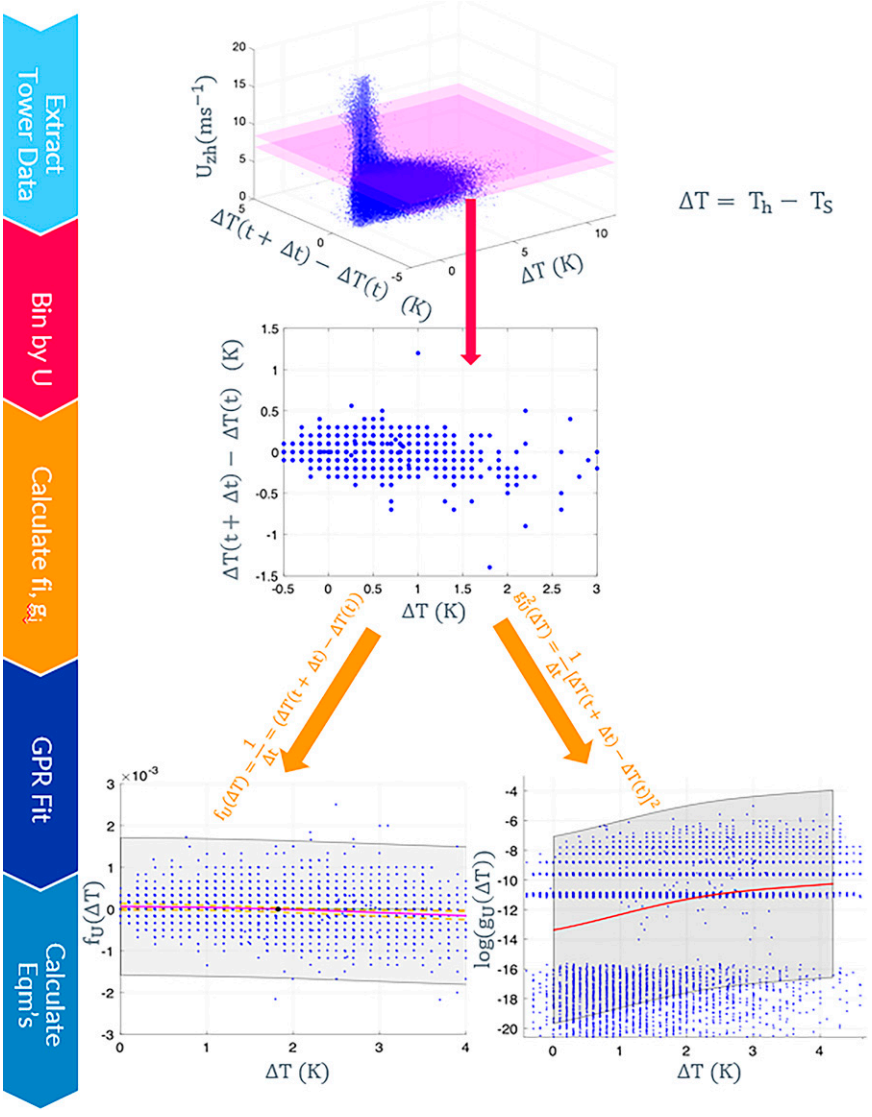


FIG. 1. A schematic of the method used to estimate empirical stochastic models. Wind speeds at the velocity crossing point and the tendency of temperature inversion measurements are extracted from meteorological towers at night. Measurements are binned by wind speed. Values of the drift $f_U$ and diffusion $g_U$ coefficient are calculated using finite differencing of the temperature inversion time series and Eqs. (7) and (8) for each wind speed bin. These finite-differenced values are fit to separate GPR models $\widehat{f_U}$ and $\widehat{g_U}$ within each wind speed bin. Equilibrium values for each wind speed bin are calculated as the zeroes of $m_f(\Delta T)$ creating an empirical bifurcation diagram.

MATLAB's fitgpr algorithm is used to fit the GPR models. GPR parameters ($\sigma_f$, $\sigma_n$, and $l$) for the squared exponential kernel [Eq. (9)] and basis function parameters are optimized by maximizing the log likelihood, $\log P(\hat{f}_U|\Delta T_u, \boldsymbol{\theta}, \boldsymbol{\beta})$ and similarly for $\hat{g}_U$. For the first $U$ bin considered for the drift $\hat{f}_U$, the initial guesses for $\sigma_f$ and $\sigma_n$ are the standard deviation of drift estimates, $[\mathbf{X}(t_{n+1}) - \mathbf{X}(t_n)]/\Delta t$, in this $U$ bin. The first guess value of the length scale $l$ is the standard deviation of input data points $X(t_n)$. For subsequent $U$ bins, the optimized GPR parameters from the previous $U$ bin fit are used to initialize the optimization. The same approach is used for the estimate of the conditional diffusion $\hat{g}_U$. All data points are used to fit the GPR. Initial tests showed GPR fits extrapolate poorly outside of the observed values $\mathbf{X}$. To avoid poorly constrained parts of the GPR fits, extracted drift and diffusion functions are restricted to the range of values within the 2.5th and 97.5th percentiles of observed $\mathbf{X}$ values in each $U$ bin.

The dynamic equilibrium temperature inversion value(s) $\mathbf{X}_{\text{eqm}}$ at each of the $N_U$ bins are computed as the zeroes of the estimated mean of the drift coefficient $m_f(\Delta T)$. The dynamic

stability of each equilibrium point is assessed using the sign of $\partial m_f(\Delta T)/\partial \mathbf{X}$ at the zero. Uncertainties in the position of equilibria are assessed by calculating the range of equilibrium values obtained for 100 realizations of the GP, computed using Eq. (10). The fraction of realizations in which a zero occurs is calculated during the uncertainty estimation. In cases where multiple zeroes occur in the mean GP, the zeroes obtained from the generated realizations are associated with the closest zero of the mean GP.

A variety of explicit basis functions to define prior expectations of the mean of $\hat{f}_U$ were explored in Ramsey (2021). A third-order polynomial basis expressed in terms of Legendre polynomials was found to produce the most robust results, particularly in cases with limited data. To ensure nonnegativity of $\hat{g}^2$ from Eq. (8), rather than modeling $\hat{g}^2_U$ directly, a model for $\hat{s}_U$, where $\hat{g}^2_U = \exp(\hat{s}_U)$ is used to fit the GPR. A constant basis function for $\hat{s}_U$ is used to allow $m_g(\Delta T)$ to be variable. The procedure described above is used to create empirical equilibrium diagrams of the SBL temperature inversion dynamics at meteorological towers around the world. The subsequent section uses the vdW17 model to explore the sensitivities of this methodology to various parameter choices and its robustness to violations of some of the underlying assumptions.

## 3. Analysis of idealized model realizations

### *The idealized model*

To test the accuracy, sensitivity, and robustness of the method for extracting effective low-dimensional stochastic dynamics of SBL temperature dynamics, described in section 2, we conduct an analysis of simulations from the nondimensionalized vdW17 model [Eq. (6)].

In the original formulation of the vdW17 model [Eq. (1)], $U$ is held constant. To account for the fact that $U$ is not constant in observations, we model this variability. Normalized fluctuations in along-wind $\hat{u}$ and crosswind components $\hat{v}$ are represented as independent, unit-variance Ornstein–Uhlenbeck processes with a common autocorrelation $e$-folding time scale $\widehat{\tau_U}$. The autocorrelation time scale is chosen to be larger than the linearized dynamic time scales of the vdW17 model so that $U$ is slowly varying and therefore equilibria are meaningful in an approximate sense, similar to the arguments made by Kaiser et al. (2020). The normalized along wind component $\hat{u}$ varies about a mean $\overline{U}$ and the mean of $\hat{v}$ is zero. The standard deviation of $U$ is then scaled by a parameter $\eta_U$. The resulting equations are

$$\begin{aligned} \frac{d\hat{u}}{ds} &= \frac{-\hat{u}}{\widehat{\tau_U}} + \sqrt{\frac{2}{\widehat{\tau_U}}}\dot{w}, \\ \frac{d\hat{v}}{ds} &= \frac{-\hat{v}}{\widehat{\tau_U}} + \sqrt{\frac{2}{\widehat{\tau_U}}}\dot{w}, \\ \hat{U} &= \eta_U\sqrt{(\overline{U}+\hat{u})^2 + \hat{v}^2}. \end{aligned} \tag{12}$$

Wind speed modeled in this way is a reasonable approximation to observations of geostrophic wind variability over land as discussed in Monahan (2014). While true winds are affected by SBL regime transitions, such effects are ignored in this highly simplified model as wind is only considered at the velocity crossing point, where tendencies associated with boundary layer processes should be weakest relative to large-scale processes. The sensitivity of empirical reconstructions to the ratio of the time scale of wind variability $\widehat{\tau_U}$ to the dynamic time scale of the model is considered later in this section. Realizations of the vdW17 model are generated using a forward Euler approximation with time step $\Delta t$. Parameters used for this model are summarized in Table 1. Subsequent sections describe the empirical estimation methods ability to reconstruct the equilibrium curve and diffusion coefficients of various model outputs.

#### 1) CABAUW-LIKE PARAMETER SET

We first consider simulations from the nondimensionalized vdW17 model with parameter values for Eqs. (6) and (12) that produce a scatterplot of $x$ versus $\hat{U}$ similar to observations at Cabauw (vdW17; Abraham and Monahan 2019a) with $\hat{\lambda} = 4 \times 10^{-4}$, $N = 10^5$, $\eta = 3 \times 10^{-4}$, and $\widehat{\tau_U} = 3 \times 10^6$. Model output is generated with a time step of 30 nondimensional time units, and subsampled every 10 points giving a sample time discretization of 300. The number $N$ of synthetic observations from model realizations is chosen to be similar to tower dataset sizes. The estimated probability distribution, conditional on $\hat{U}$, of an example model realization is shown on the left side of Fig. 2. Also shown is the equilibrium structure for this model realization obtained using a pseudoarc-length continuation algorithm (Dijkstra et al. 2014).

The linear dynamical time scale of the vdW17 model,

$$\tau_{x(\hat{U})} = \left\{\frac{\partial}{\partial x}\left[\hat{Q} - \hat{\lambda}x - c_d\hat{U}f\left(\frac{x}{\hat{U}^2}\right)x\right]\right\}^{-1}\Bigg|_{x(\hat{U})=x_{\mathrm{eq}}(\hat{U})}, \tag{13}$$

can be obtained from the coefficient of dynamics linearized about the equilibrium solution for fixed $\hat{U}$ as shown for the Cabauw-like parameter values on the right side of Fig. 2. The linearized dynamical time scale provides an estimate of the time required by the system to return to equilibrium. The upper branch of the equilibrium solution at low $\hat{U}$, high $x$ (which we associate with the vSBL) has a larger $\tau_{x(\hat{U})}$ than the lower branch of the equilibrium solution at large $\hat{U}$, low $x$ (which we associate with the wSBL). It is therefore expected that in the modeled wSBL, the system will adjust to perturbations away from equilibrium relatively quickly. A spike in $\tau_{x(\hat{U})}$ occurs where the system transitions between branches, around $\hat{U} \approx 0.5$. The long linear adjustment time scale of $x$ over a small window of $\hat{U}$ is related to a critical slowing indicating that the system is close to a bifurcation point (Scheffer et al. 2009). For other sets of model parameters, an unstable equilibrium appears between the upper and lower equilibrium branches, producing a pair of back-to-back fold bifurcation (discussed further below). The magnitude of the spike becomes infinitely large at the bifurcation points.

For the empirical reconstruction of the dynamics, $N_U = 50$ $\hat{U}$ bins are used, as discussed in section 2. The estimated equilibrium structure is plotted in the first two panels of the top row of Fig. 3; the true equilibrium curve is included in the

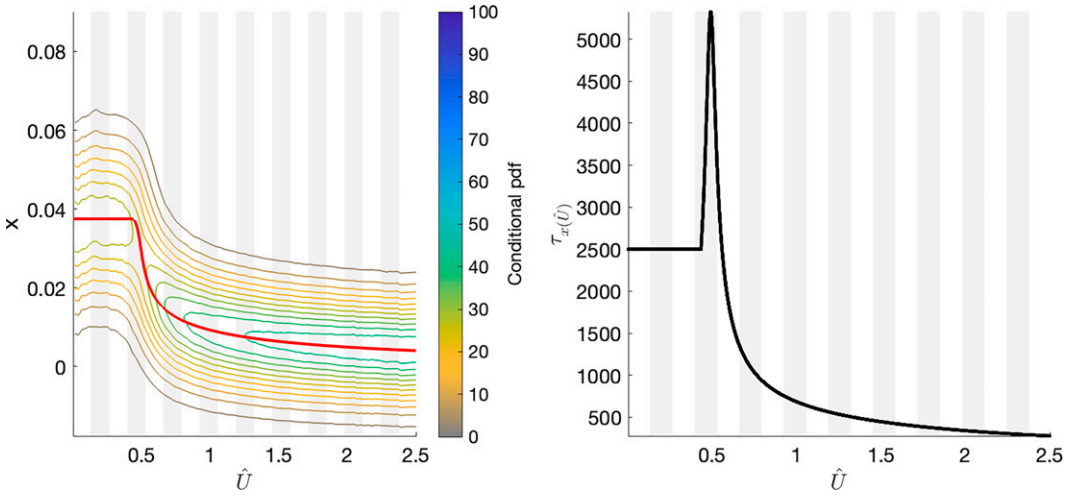


FIG. 2. (left) Contours show kernel density estimates of the probability density function of nondimensionalized model output with additive noise [Eq. (6)] conditioned on wind speed $\hat{U}$ using parameters from Table 1 with $\hat{Q} = 1.5 \times 10^{-5}$, $\hat{\lambda} = 4 \times 10^{-4}$, $\sigma = 3 \times 10^{-4}$, $\hat{\tau_U} = 3 \times 10^6$ and $N = 10^6$. The red curve shows the deterministic equilibrium structure for fixed values of $\hat{U}$. (right) The linearized dynamic adjustment time scale $\tau_{x(\hat{U})}$ of nondimensionalized model output with no noise [Eq. (4)], using these parameter values. Alternating gray and white bands panels in the background show the $\hat{U}$ bins used for the estimation method.

second panel. Estimated equilibrium points from model simulations clearly follow the true deterministic equilibrium structure. Equilibria at all values of $\hat{U}$ are correctly found to be dynamically stable. True equilibria all lie well within the range of uncertainty computed for estimated equilibria. The estimated $\hat{g}_U$ for this model realization is shown in the third panel of the top row of Fig. 3. Note that $\hat{g}_U$ values are fit separately over each $\hat{U}$ bin so there is uncorrelated sampling variability between $\hat{U}$ bins. Because model noise is additive in this case $\hat{g}_U$ should be the constant value $3 \times 10^{-4}$. Reconstructed values are generally close to the true value, although $\hat{g}_U$ values in the wSBL region are biased slightly low.

It is clear from the top row of Fig. 3 that the estimation procedure is able to reasonably reconstruct the bifurcation structure and the diffusion coefficient of the vdW17 model with the Cabauw-like parameters. The sensitivity of reconstructed dynamics to changes in parameter values and data processing is explored in subsequent subsections.

### 2) MULTIPLE EQUILIBRIUM PARAMETER SET

It was hypothesized in vdW17 in some locations (such as Dome C, Antarctica) that spontaneous SBL regime transitions are associated with a pair of back-to-back fold bifurcations. It is therefore important to test that our method is able resolve multiple equilibria. The ability of this approach to reconstruct idealized model dynamics for parameters showing multiple equilibria is examined by decreasing the nondimensionalized surface exchange coefficient to $\hat{\lambda} = 8 \times 10^{-5}$ (Fig. 3, second row), representing poor insulators, like ice. At this lower value of $\hat{\lambda}$ an unstable branch exists between approximately $\hat{U} = 0.5$ and $\hat{U} = 1$, implying the occurrence of spontaneous transitions between SBL regimes as slowly changing $\hat{U}$ passes a bifurcation point. Because the intermediate branch is unstable, the number of points close to this branch are small in the simulations. On the unstable branch the effective dynamic time scale is negative as the equilibrium repels solutions, making it more difficult for the method to find equilibrium values. Nevertheless, the overall equilibrium structure over the unstable branch is reconstructed. The dynamical stability of points is properly determined for the most part, and the diffusion $\hat{g}_U$ is reasonably well recovered. The sensitivity of the method to length of the time series is explored in Ramsey (2021), showing that datasets of approximately $N = 10^5$ are sufficient for this reconstruction procedure. The sensitivity of the method to how the data are processed by time averaging is subsequently explored.

### 3) TIME AVERAGING

The time averaging of the different datasets considered in this study varies between locations. The observational datasets considered in section 4 represent time averages over intervals varying from 1 to 30 min, depending on the tower considered. Because our analysis is investigating effective low-dimensional dynamics, some time averaging of observations is important, as will be shown for the Hamburg dataset in section 4. Averaging over periods that are too long can however obscure the dynamics. By construction, the vdW17 model output considered in this section for comparison represents time averaged quantities. We consider the effects of excessive time averaging on the reconstructed dynamics by averaging model realizations across 10 point intervals. A realization from the multiple equilibrium parameter set considered above, initially with $N = 10^6$ points, is used to assess the impact of time averaging on unstable equilibria. After averaging, the dataset has $N = 10^5$ points.

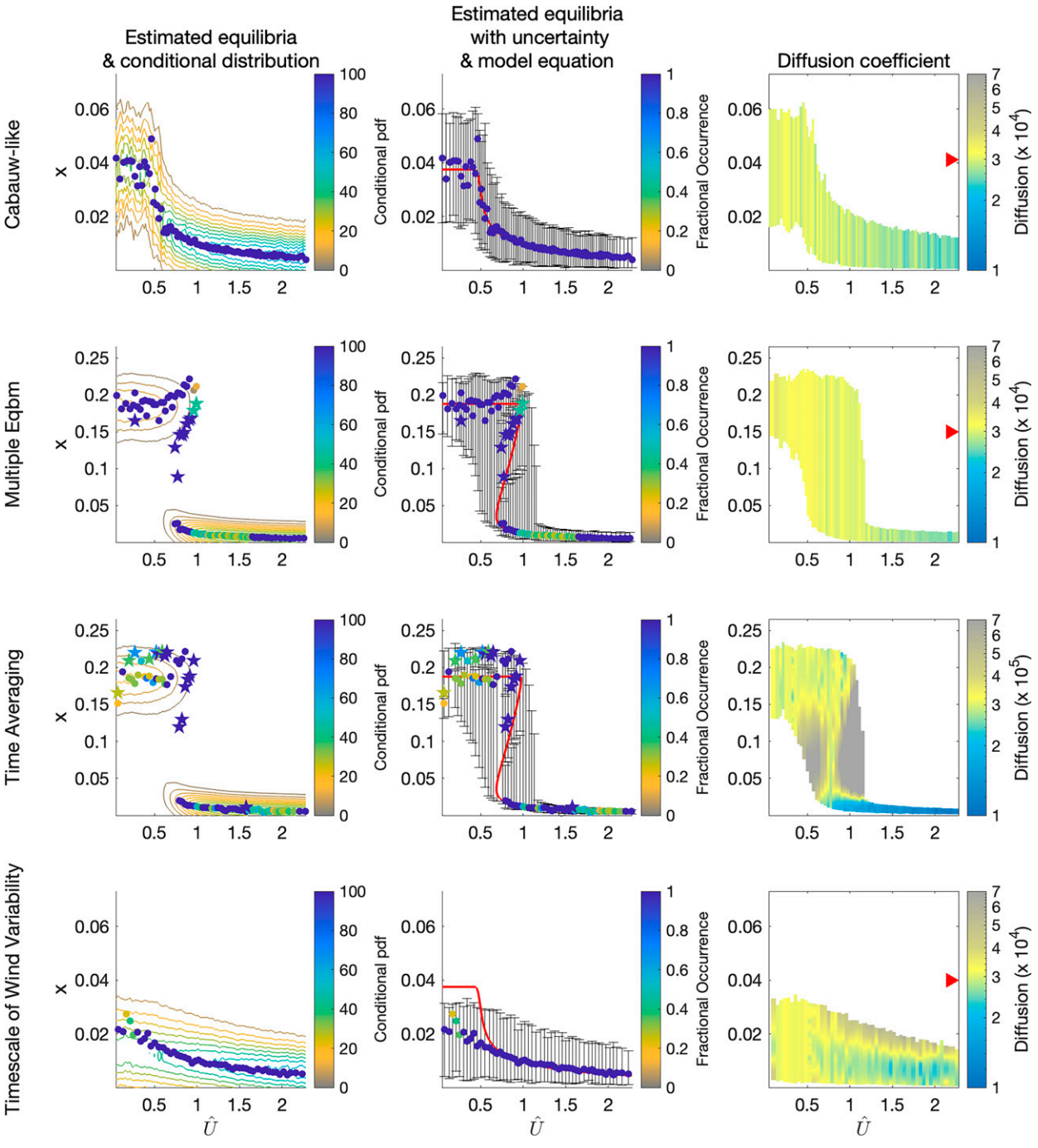


FIG. 3. Empirically estimated equilibria (points). Dynamically stable equilibria are shown as circles and dynamically unstable equilibria are shown as stars. The color of points indicates the fraction of times different realizations of the GPR find an equilibrium point over the range of data. Each row represents a different analysis (described in detail in section 3), as identified in titles to the left. (left column) Kernel density estimate of various realizations of the nondimensionalized model with additive noise [Eq. (6)]. (center column) Estimated equilibrium values along with their 2.5th- and 97.5th-percentile uncertainty ranges. The red curve shows the deterministic equilibrium curve of the model. (right column) Estimated diffusion coefficients.

The estimated equilibrium structure obtained from the 10-point-averaged model realization is shown in the third row of Fig. 3. The estimation procedure continues to find equilibrium points along the stable branches; however, fewer unstable points along the unstable branch are resolved when compared to the nonaveraged data in the second row. Multiple unstable equilibria on the upper, vSBL equilibrium branch are incorrectly identified.

The diffusion coefficient obtained from 10-point-averaged data is shown on the rightmost column of Fig. 3. The overall magnitude of $\hat{g}_U$ decreases by at least a factor of 10, due to the time averaging acting as a low-pass filter on high-frequency noise. Reconstructed $\hat{g}_U$ values in the vSBL are higher than those in the wSBL. This result is consistent with the fact that $\tau_{x(\hat{U})}$ is higher for the vSBL than in the wSBL (Fig. 2). We interpret the larger $\hat{g}_U$ in the vSBL to be a result of relatively low-frequency vSBL variations being less affected by the low-pass filtering due to time averaging. We therefore find that excessive time averaging results in different diffusivity estimates in the vSBL than in the wSBL. The appearance of diffusivity varying with state variables due to time averaging results in a spurious interpretation of the presence of multiplicative noise. The large positive bias on the edges of the unstable branch is likely due to the sparsity of data in this region. The sensitivity of the method to nonstationarity of wind speeds is subsequently explored.

#### 4) TIME SCALE OF WIND VARIABILITY

Implicit in the reconstruction procedure is the assumption that $U$ varies over sufficiently long time scales relative to $\Delta T$ so that $U$ can be taken as quasi stationary within each $U$ bin. In nature, both $U$ and $\Delta T$ vary within the night. To test the method's sensitivity to this assumption, calculations are repeated for simulations generated across a range of values of wind fluctuation memory $\widehat{\tau_U}$. For this analysis, the Cabauw-like set of parameter values are used. Plots of the reconstructions from model realizations with $\widehat{\tau_U} = 1000$ which is comparable to the time scale of the linearized dynamics of the vdW17 model for the Cabauw-like parameters (Fig. 2) are shown in the bottom row of Fig. 3.

It is clear that that for $\widehat{\tau_U}$ close to the typical scale of $\tau_{x(\hat{U})}$, the reconstruction of the equilibrium structure is less accurate. Estimated values deviate from the true equilibrium in the vSBL, where the linearized dynamical time scale is the largest. Tests at slightly larger $\widehat{\tau_U}$, however, show that the reconstruction is reasonably accurate even when $\widehat{\tau_U}$ is not much larger than the typical value of $\tau_{x(\hat{U})}$ (Ramsey 2021). In observation-based reconstructions, variability of the true $U$ may bias the estimated equilibrium structure if $\hat{\tau_U}$ is not at least a few times longer than $\tau_{x(\hat{U})}$. It is however difficult to estimate the value of $\tau_{x(\hat{U})}$ from observations as the conceptual model depends on many parameters that are difficult to accurately constrain observationally.

Estimated $\widehat{g_U}$ for model realizations with $\widehat{\tau_U} = 1000$ also show a reduction in reconstruction accuracy when the wind varies on a time scale comparable to the time scale of the linearized dynamics. In particular, a more pronounced quadratic bias appears as $\widehat{\tau_U}$ approaches $\tau_{x(\hat{U})}$.

Our analysis has also held the isothermal net radiation $\hat{Q}$ constant, when in fact it can also vary over the night (particularly due to changes in cloud cover). Because this term is not taken to be state dependent, variations in $\hat{Q}$ will manifest as enhanced values of the diffusion coefficient.

Sensitivity tests show that the empirical estimation method is able to reconstruct the dynamics of the nondimensionalized vdW17 model with additive white noise, so long as the data are not excessively time averaged and variations of wind speed are sufficiently slow. The effective low-dimensional dynamics extracted using this method on data from five different meteorological towers around the world is now explored.

## 4. Tower data

Time series data from five different land-based meteorological towers are used to investigate the low-dimensional effective dynamics of SBL temperature inversions using the method described in section 2 and illustrated for the vdW17 model in section 3. Detailed information about these datasets is provided in Abraham and Monahan (2019a); a summary is presented in Table 2. Information about data availability can be found in the acknowledgments. The towers are located around the world in a range of locations with varying meteorological settings and surface conditions. Cabauw, Netherlands, is located on flat, moist agricultural land with relatively limited surrounding topography or urban development. The Hamburg tower is located on similarly flat, moist grass land in a river valley, 8 km from the urban metropolis of Hamburg, Germany. Dome C is located on flat terrain in the interior of Antarctica, providing insight into SBL dynamics in ice-based conditions. The Karlsruhe tower is located in a small clearing of a forested valley, 10 km from the city of Kalrsruhe, Germany. Los Alamos is located on a very dry plateau downslope of the Jemez Mountains in New Mexico, United States. Data from the Boulder tower considered in Abraham and Monahan (2019a,b,c) are not considered because the lowermost observational level is too high to properly characterize the temperature inversion. For this study, an energetically based definition of nocturnal data is used when possible, defining night as those times with the net radiative flux density $Q_{\text{net}} < 0$ when such measurements are available. At stations where radiative flux measurements are not available, data 2 h before sunset and sunrise are used, as in Abraham and Monahan (2019a). Van Hooijdonk et al. (2017b) analyzes the growth rate of temperature inversions around sunset at a number of land meteorological tower and concludes that development of the SBL begins 2 h prior to sunset. Because this study is not interested in transitional periods a more conservative choice of 1 h is used. Cabauw offers the most comprehensive dataset and is therefore examined first.

### a. Cabauw

We now analyze time series from the tower in Cabauw. A comprehensive review of this site can be found in Bosveld et al. (2020). Temperature and wind speed measurements from 2001 to 2019 Reynolds averaged over 10-min intervals are considered (Van Ulden and Wieringa 1996). Based on previous analyses, we take $z_h$ to be at 40 m (van de Wiel et al. 2012a). Results considering $U$ and $\Delta T$ for other measurement heights are considered in Ramsey (2021). Here, $\Delta T$ is calculated between 2 and 40 m.

The reconstructed equilibrium temperature inversion $\Delta T_{\text{eqm}}$ values conditioned on $U(z_h)$ are plotted as a function of binned $U(z_h)$ in Fig. 4. The estimated $\Delta T_{\text{eqm}}$ clearly follow a sigmoidal equilibrium structure similar to that of the vdW17 model, with large $\Delta T_{\text{eqm}}$ at low $U(z_h)$, and small $\Delta T_{\text{eqm}}$ at

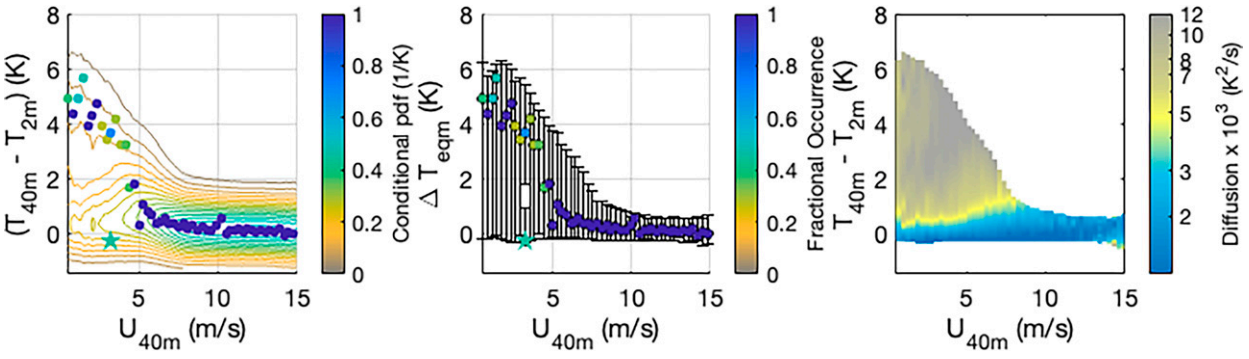


FIG. 4. (left) Contours of the kernel density estimate of temperature inversion as a function of wind speed from the Cabauw Meteorological data tower at a height of 40 m. (center) Reconstructed equilibrium values along with uncertainties (expressed as the 2.5th–97.5th-percentile ranges). (right) The estimated diffusion function. Note that contours extend to statically unstable values of the stratification because of the width of kernel used in the estimation of the pdf; such points are not used in the analysis.

large $U(z_h)$, similar to results from the nondimensionalized model results in section 3. The single unstable equilibrium point found for $\Delta T_u < 0$ is not robust to modest changes in the estimation procedure. The estimated diffusion coefficient from the GPR fit to the Cabauw 40 m dataset is also shown in Fig. 4. A clear structure of much smaller diffusion in the wSBL and larger diffusion in the vSBL is evident. This systematic variation in diffusion coefficient values strongly suggests the existence of multiplicative noise in this system, consistent with observations of submesoscale processes and intermittent turbulent bursts in the vSBL (van der Linden et al. 2020; van de Wiel et al. 2003). The transitional zone between the vSBL and wSBL occurs around $U(z_h) = 5$ m s$^{-1}$, as suggested by other lines of evidence of Cabauw (van Hooijdonk et al. 2015; van de Wiel et al. 2012b; Abraham and Monahan 2019a).

It is noteworthy that the estimated equilibria do not simply track the maxima of the pdf of $\Delta T$ conditioned on $U(z_h)$, particularly in the vSBL, where the $\Delta T_{\text{eqm}}$ values are far greater than the most frequently observed values. This result differs from those found for the idealized model using additive noise.

Ceilometer measurements reporting the percentage of cloud cover were taken at Cabauw from June 2008 to April 2017. While this data record is shorter than the tower temperature and wind measurements its analysis provides insights into the effects of clouds on SBL regime occupation. We characterize low-level cloud cover (LLCC) less than 20% as clear sky ($N = 9 \times 10^4$ data points) and LLCC greater than 20% as cloudy ($N = 1.5 \times 10^5$ data points). The cloudy and clear-sky datasets are then analyzed separately (Fig. 5).

The estimated equilibrium structures under both cloudy and clear-sky conditions show equilibrium structures broadly similar to those obtained at Cabauw using the entire record. The structures, however, differ in detail. Clear-sky conditions show stronger temperature inversions and a sharper transition between regimes. Cloudy conditions show weaker vSBL temperature inversions and more gradual transitions between SBL regimes. The transition $U(z_h)$ under cloudy conditions (~5 m s$^{-1}$) is slightly lower than the transition $U(z_h)$ under clear-sky conditions (~6 m s$^{-1}$), as found in Abraham and Monahan (2019b) and Monahan et al. (2015). This is in keeping with the finding in Acevedo et al. (2021) that the transition wind speed $U(z_h)$ increases with net radiative loss. Diffusion coefficient plots show slightly increased noise for small $U$ and small $\Delta T_u$ under clear skies relative to cloudy conditions (Fig. 4), although the sparsity of data available makes it difficult to interpret these results with confidence. Other than this difference the diffusion structures are similar under clear and cloudy skies. We now explore the effective low-dimensional dynamics of the SBL in a high-latitude setting.

## DOME C

We now consider time series data from Dome C, located on the East Antarctic Plateau. The meteorological tower is located on a flat snow surface, 900 km from the coast. The flat terrain results in relatively weak katabatic winds. Large-scale, dry southerly winds dominate resulting in predominantly clear-sky conditions. Strong temperature inversions form due to strong radiative cooling during polar nights and large-scale subsidence. A detailed description of this site can be found in Genthon et al. (2021) and Vignon et al. (2017a,b). Because snow and ice are good insulators, relatively weak surface exchanges of energy occur. The effective surface coupling parameter $\lambda$ for this site is therefore expected to be the lowest among the sites considered. From the perspective of the vdW17 model, this location is therefore the most likely to show backfolding of the equilibrium structure. While scatterplots of observed $\Delta T$ against $U$ in vdW17 and Vignon et al. (2017b) suggests the existence of multiple equilibria at Dome C, the effective dynamics of the SBL are not quantitatively explored in those studies. Temperature, radiation, and wind speed measurements from 2011 to 2018, Reynolds averaged over 30 min intervals, are used in this analysis. The relatively large averaging interval and shorter observational period at this site make it the smallest of the datasets considered, with $9 \times 10^4$ data points. Therefore, $N_U = 30$ is used. The 9-m measurement height is taken as $z_h$ in keeping with the estimates of velocity crossing point in Vignon et al. (2017a,b). Two alternative measurements are considered for the lower-

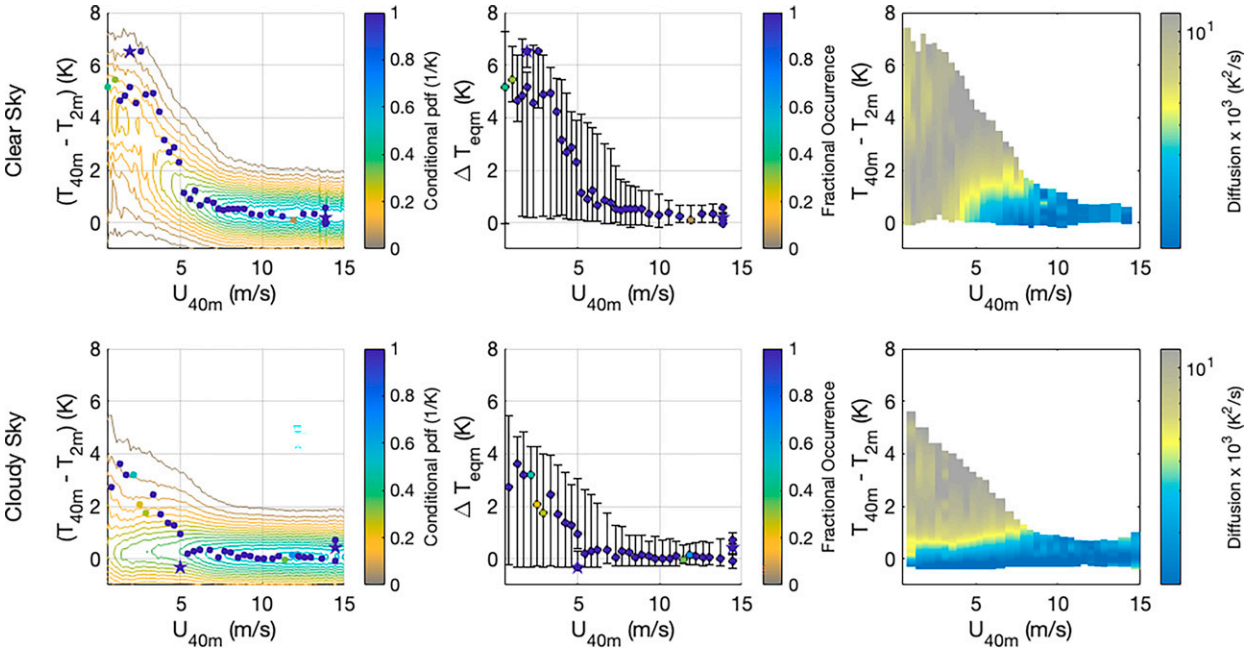


FIG. 5. (top) As in Fig. 4, but for clear-sky data from Cabauw (LLCC < 20%). (bottom) As in Fig. 4, but for cloudy conditions at Cabauw (LLCC ≥ 20%).

altitude temperature: the 1.3 m thermometer measurement and the surface temperature derived from longwave radiative fluxes. As described in Vignon et al. (2017a), the surface temperature can be calculated using measurements of upwelling and downwelling longwave radiative flux measurements, $LW_{up}$ and $LW_{down}$, obtained from pyranometers. Temperature inversions calculated from longwave radiative flux produce a subset of data with large $U(z_h)$ and $\Delta T$. These results are interpreted as unphysical, since large temperature inversions cannot be maintained at high wind speeds. Furthermore this subset of points does not exist when 1.3 m is used as the lower temperature. Points with $U(z_h)$ greater than 10 m $s^{-1}$ and radiatively estimated $\Delta T$ greater than 7 K are therefore excluded from the analysis.

The resulting equilibrium structure estimated for $\Delta T$ between 1.3 and 9 m is shown in the top row of Fig. 6, and between temperatures at the surface and 9 m in the lower panels. Both estimated equilibrium structures at Dome C again show sigmoidal structures broadly similar to the Cabauw data (Fig. 4). Similar equilibrium structures are estimated for inversions calculated using surface temperatures derived from longwave radiative flux as using 1.3-m temperature measurements. Equilibrium temperature inversion values are higher for radiative flux derived temperatures than for 1.3-m bottom temperatures as a result of the large temperature gradient near the surface. As at Cabauw, equilibria follow the maximum of the pdf only at large $U$. At low and intermediate $U$, estimated equilibria occur at $\Delta T$ values much larger than the maxima of the conditional pdf.

The transition between regimes occurs around $U \sim 6$ m $s^{-1}$, consistent with the critical wind speed derived from the MSHF framework in Vignon et al. (2017b). The transitional region, between large $\Delta T$ at low $U$, and low $\Delta T$ at large $U$, occurs more abruptly than at Cabauw, and is accompanied by equivocal evidence of multiple equilibria. The distribution of equilibria in the transitional region shows evidence of backfolding, with a few unstable equilibrium values. However, the number, position, and dynamical stability of equilibria in the transitional region vary depending on the lower-level temperature used and number of $U$ bins. As shown in section 1, the estimation procedure has difficulty resolving backfolding equilibrium branches, particularly in datasets with relatively few points and averaged over relatively long intervals, as is the case at Dome C. These results provide suggestive but not definitive evidence for the existence of multiple equilibria and dynamically unstable states in the SBL surrounding Dome C. A few unstable equilibria also appear at high $U$ and low $\Delta T$, inconsistent with the vdW17 model, which further decreases our confidence in the interpretation of evidence of multiple equilibria at Dome C. Kaiser et al. (2020) argue that the relatively long averaging time scale of these data (30 min) approaches the time scale of SBL dynamics and biases the results of the empirical reconstruction of the dynamics (as shown for the vdW17 model in section 3). Higher-frequency observations would be expected to improve the accuracy of the reconstructed dynamics at this site.

The estimated diffusion coefficients obtained for $\Delta T$ calculated with a base of 1.3 m and from longwave radiative flux estimates of surface temperature are shown in Fig. 6. While results are noisy, both show increased noise at large $\Delta T$, under which conditions intermittent turbulent bursts have been observed to occur (Petenko et al. 2019; Baas et al. 2019). Intermittent turbulent bursts observed at Dome C have been related to Kelvin–Helmholtz instabilities resulting from

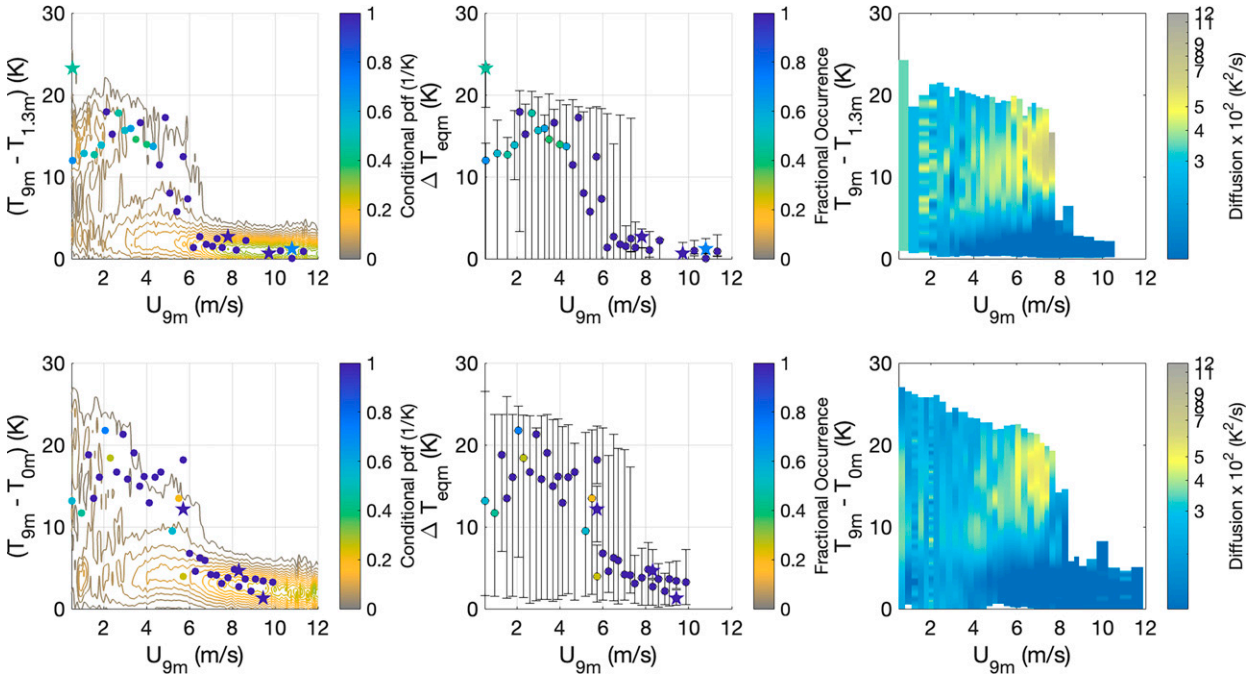


FIG. 6. (top) As in Fig. 4, but for Dome C temperature inversions calculated between 1.3- and 9-m measurement heights. (bottom) As in Fig. 4, but for Dome C for temperature inversions calculated using longwave radiative flux and the 9-m measurement height.

accelerating winds aloft and decelerating surface friction produced in LES models (van der Linden et al. 2020). We now explore a dataset with a higher temporal resolution to explore in an observational setting the extent to which the time-averaging interval affects extracted dynamics.

### b. Hamburg

The Hamburg data tower reports values Reynolds averaged over 1 min intervals, in contrast to the 10–30-min averaging intervals at other stations. This dataset therefore allows investigation of the effects of the averaging interval on results. The equilibrium structures obtained for Hamburg data calculated using $z_h = 50$ m and data averaged over 10- and 1-min averages are compared in Fig. 7.

The equilibrium curve from the 10-min Reynolds-averaged data shows a sigmoidal structure similar to that found for 10-min averaged data at Cabauw (Fig. 4). The 1-min Reynolds-averaged data show a similar curve, but with substantially increased scatter and the addition of a number of dynamically unstable equilibria at low $U$ and low $\Delta T$. These equilibrium states are not physically plausible. In particular, they are inconsistent with the surface energy budget expressed by the idealized model introduced in section 2. These points are not present in the reconstructions of the dynamics using 10-min averaged data, suggesting that at the relatively fine resolution of 1-min averages, the approximation of the inversion dynamics as an effective low-dimensional dynamical system is no longer reasonable. Effective low-dimensional dynamics for this system appear to be more appropriate on time scales of 10–30 min. The 1 min Reynolds-averaged data also estimate unstable equilibria in the transitional region. However, because so many unrealistic equilibria are also estimated, the existence of such dynamically unstable states cannot be concluded with any confidence.

The estimated diffusion coefficients for the 1- and 10-min Reynolds-averaged data are also shown in Fig. 7. Once again, clear evidence of multiplicative noise, with enhanced noise strength in the vSBL is found for the 1- and 10-min averaged data. This structure is also found when the Hamburg data are averaged to 30 min (Ramsey 2021). A notable difference between the diffusion plots is that the diffusion magnitude of 1 min Reynolds-averaged data is much larger than that of the 10- and 30-min Reynolds-averaged data, similar to time averaged vdW17 model results in section 3. This result is consistent with the interpretation that averaging reduces the signal from short time scale processes not represented by the deterministic system considered and therefore manifesting as noise. However, a large contrast in noise strength between the vSBL and wSBL exists for all averaged datasets, providing evidence that the enhanced noise strength in the vSBL is not an artifact of time averaging as found for the idealized model in section 3. We now compare results at all five meteorological towers considered.

## COMPARISON OF ALL STATIONS

The estimated equilibrium structures for all meteorological towers considered (with Hamburg data averaged to 10 min) are shown in Fig. 8. All towers show the sigmoidal equilibrium structure suggested by the vdW17 model. As the estimation procedure described in section 2 imposes no assumption on the form of the equilibrium structure, these results provide empirical evidence that the vdW17 model captures essential

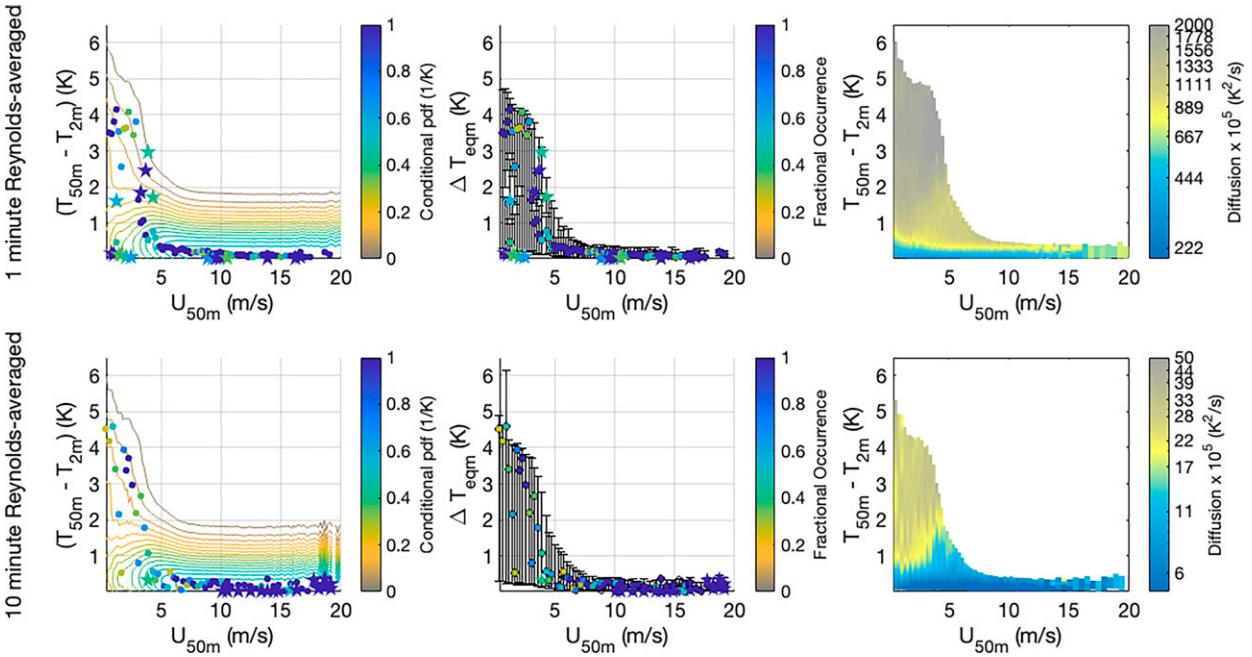


FIG. 7. (top) As in Fig. 4, but with 1-min-resolution data for Hamburg. (bottom) As in Fig. 4, but with data averaged over 10-min intervals for Hamburg.

low-dimensional features of SBL dynamics. The transitional $U$ range between the vSBL and wSBL occurs over a broader range of lower wind speeds at Los Alamos and Cabauw than at Dome C. The estimated diffusion coefficient plots for all towers are shown in Fig. 9. At all sites, diffusion values are considerably lower in the wSBL than in the vSBL. The diffusion structures are broadly similar between sites.

Further work accounting for wind speed variations, the effects of data averaging and multiplicative noise modeling is required to determine the extent to which actual SBL dynamics display hysteretic structures such as those predicted by the vdW17 model. Incorporating the early warning system metric proposed in Kaiser et al. (2020) to filter $U$ for times at which the system appears to be approaching an unstable state may help facilitate this. Alternative semiparametric SDE estimation methods such as the statistical inference model approach propose in Krumscheid et al. (2015) and the variational clustering approach proposed in Boyko et al. (2021) could also be explored in future work.

## 5. Discussion and conclusions

A primary goal of this study has been to investigate how well the SBL inversion dynamics can be expressed as a low-dimensional dynamical system, inspired by the vdW17 model, with the inclusion of a stochastic term representing processes not explicitly represented by this low-dimensional approximation. Evidence of the effectiveness of such a low-dimensional approximation provides strong evidence that vdW17 captures essential physical controls on SBL regime dynamics—in particular the important influence of surface energetic coupling on the bifurcation structure. The estimated equilibrium structures at five tower sites around the world show the sigmoidal equilibrium structure predicted by the vdW17 model. The equilibrium structures differ in detail between the five sites due to differences in measuring altitudes, averaging time, record length, quantities measured, and local conditions. Importantly, these differences also appear to reflect the role of surface energetic coupling as predicted in vdW17. Equilibrium values at all sites do not simply follow the observed maximum probability distribution (conditioned on wind speed $U$) in the vSBL region, where noise is found to be state dependent. In the wSBL, however, equilibria do follow the maximum of the probability distribution. The location of the transitional $U$ range separating the vSBL and wSBL varies by location. The transitional $U$ of ~5 and ~6 m s$^{-1}$ at Cabauw and Dome C are in agreement with previous estimates by van de Wiel et al. (2012b) and Vignon et al. (2017a), respectively.

Evidence of multiple equilibria with hysteresis between vSBL and wSBL regimes is found at Dome C, although there is considerable scatter in the results and this structure is not robust to the details of the analysis. No evidence of such structure is found elsewhere. Sensitivity tests using the idealized vdW17 model show that unstable equilibria are not reliably recovered by the method we have used for data records that are too short or data averaging time scales that are too long. Furthermore, the equilibrium estimation procedure assumes wind speeds are quasi stationary within $U$ bins. In section 3 it was shown that for the vdW17 model, when wind speeds vary on shorter time scales, estimated equilibrium values are smaller and the transitional region is broader than the deterministic solutions. It is therefore possible that the weak evidence of multiple equilibria found in the tower data is a

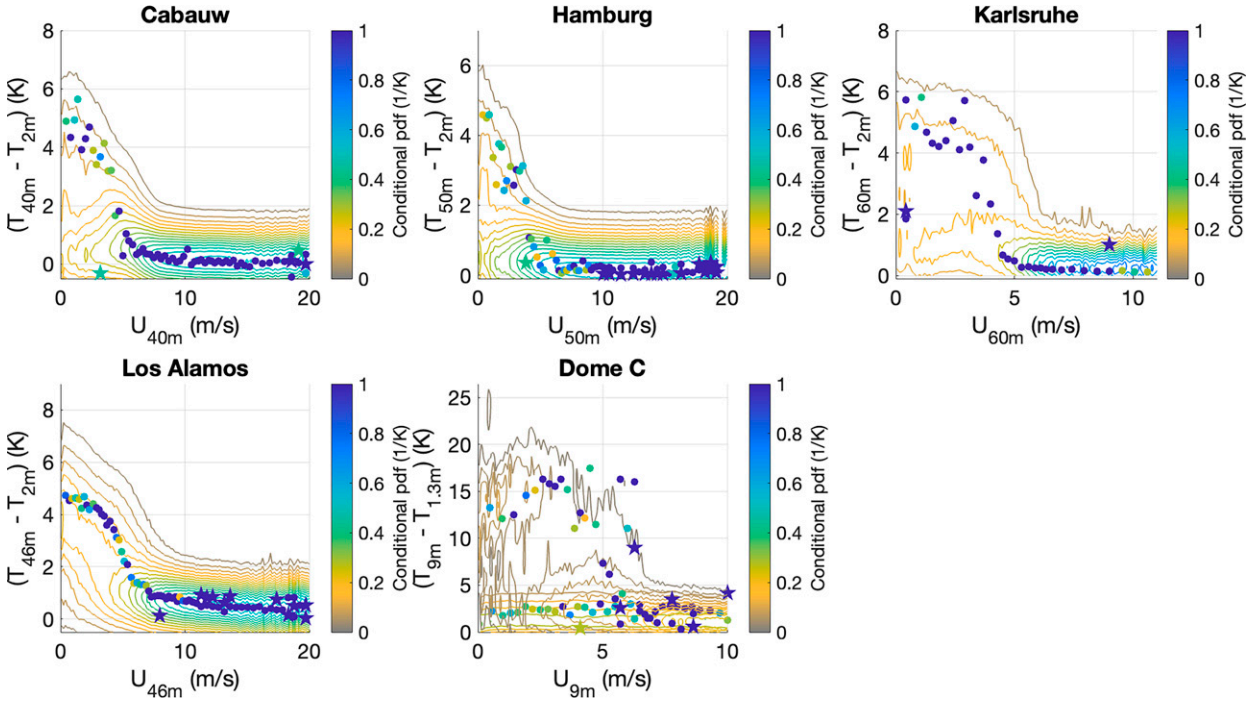


FIG. 8. Empirical equilibrium diagrams obtained for all meteorological towers considered, along with contours of the estimated inversion pdf. Symbols are as in Fig. 3.

consequence of data processing and wind speed variations. Estimating the time scale of wind speed variation at each site would provide further insights into the extent to which these results depend on the averaging scale of observations. Additional tests on the influence of treating wind speeds as quasi stationary within wind speed bins would also help contextualize results.

Estimated diffusion coefficients show increased noise strength in the vSBL at all six towers considered. This result is consistent with previous observations of enhanced submesoscale activity and intermittent turbulence in the vSBL (e.g., Abraham and Monahan 2019a; Mahrt 2014; van de Wiel et al. 2003). A fact relevant to interpreting this result is that time averaging of vdW17 model output with additive noise results in lower estimated diffusion in the wSBL than in the vSBL. Thus, the reconstructed noise appears state dependent when the true noise is additive. This result indicates that the apparent state-dependent noise intensity in the tower data could be an artifact of data processing. However, the appearance of multiplicative noise in the Hamburg data over a broad range of averaging periods provides evidence that the noise structure is not simply an artifact of time averaging. Together, these results indicate that the effective low-dimensional dynamics of the SBL should involve state-dependent noise, with stronger noise in the vSBL. This result is of particular interest in the context of modeling the role of intermittent turbulent bursts initiating SBL regime transitions in operational weather and climate models (e.g., Abraham et al. 2019).

The estimation procedure results in an SDE in Itô form; the Stratonovich form is more appropriate for a physical system with multiplicative noise (Gardiner 1990; Penland 2003). As our results suggest the existence of multiplicative noise, it is expected that the Itô drift term includes a noise induced drift, potentially influencing the reconstructed equilibrium structure. Converting results to the Stratonovich form requires calculation of derivatives of the diffusion coefficients with regards to the state variable. The fact that derivatives must be taken of potentially noisy diffusion estimates could strongly affect estimates of zeroes of the Stratonovich drift using our approach. Accounting for this noise-induced drift by smoothing estimated diffusion coefficients in order to obtain deterministic bifurcation structures without noise induced drift is an interesting direction of future study.

Kaiser et al. (2020) also used a stochastic extension of the vdW17 model to consider SBL regime occupation and transitions. Changes to ARMA fits to time series of SBL data were used to predict regime transitions and determine dynamical stability. While quasi stationarity of $U$ within a bin is not required in their analysis, a sliding time window of length such that the statistical dynamical system is in equilibrium must be specified. Kaiser et al. (2020) provided evidence of an unstable equilibrium branch and stable wSBL branch using data with 1-min resolution from a tower in Dumosa, Australia, but find no evidence of a stable vSBL branch. Considering 30-min averaged data at Dome C, they find that this time series has insufficient resolution for their methodology. Our analysis procedure does not require such high-resolution observations,

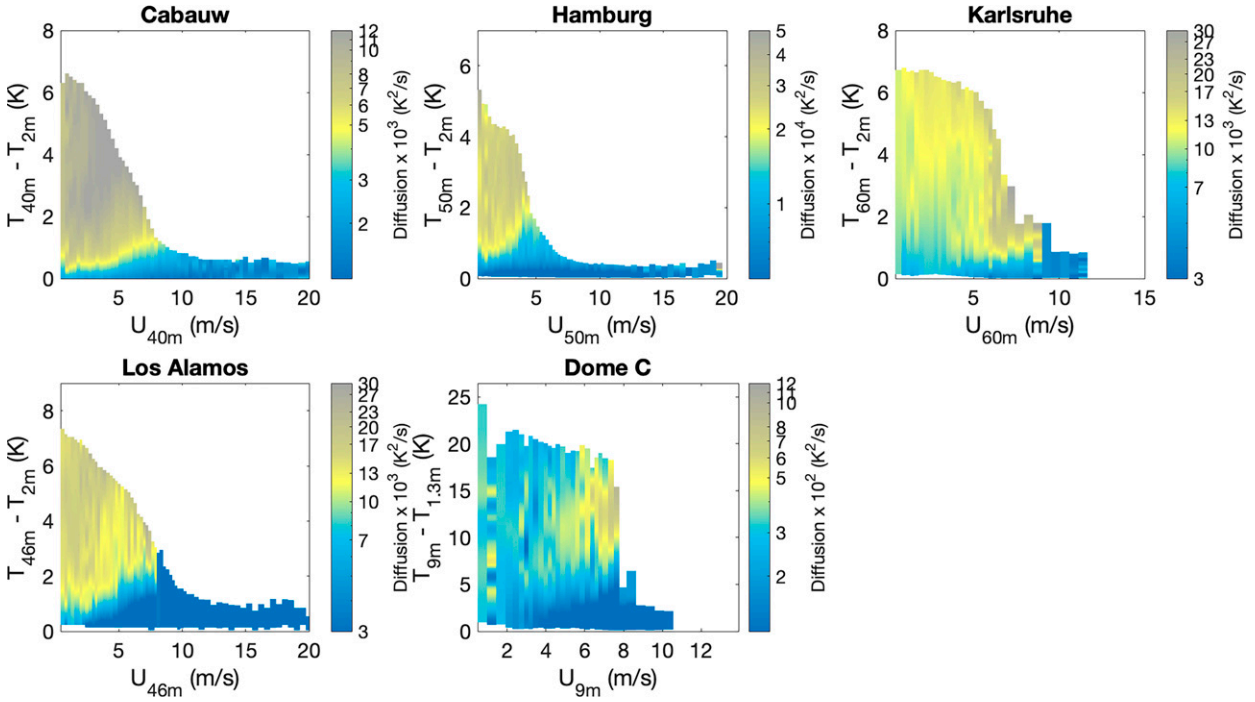


FIG. 9. As in Fig. 8, but for diffusion coefficients estimated at all meteorological towers considered in this study. Note that the range of the color bar changes across the panels.

although robust characterization of the bifurcation structure does require relatively long time series. A direct comparison of the two methods, perhaps in the context of an idealized model in which the bifurcation structure is known, is another direction of future study.

This work has demonstrated that time series of inversion strength and $U$ allow empirical reconstruction of effective low-dimensional dynamics consistent with the vdW17 model, using observational data from a range of locations around the world. While a suggestion of multiple equilibria and hysteresis behavior was presented for Dome C, Antarctica, this result is sensitive to the details of how the analysis has been conducted. We have also provided evidence of state-dependent noise in these data, with enhanced noise strength in the vSBL consistent with the presence of intermittent turbulence events. The work presented provides a quantitative analysis of the degree to which the vdW17 model is an effective representation of SBL dynamics at a range of different locations.

These results provide direct empirical evidence that the vdW17 model captures the essential elements of SBL physics, particularly if a stochastic term in included. The bifurcation behavior of the SBL temperature inversion is examined without assuming the vdW17 model specifically, empirically demonstrating the effectiveness of a low-dimensional surface energy approach to modeling SBL regime dynamics. The strength of the surface energetic coupling was identified in vdW17 as a primary control on the SBL inversion bifurcation structure, although because of the idealized nature of this model empirical estimates of the associated parameter $\lambda$ are not straightforward. The approach taken in this study allows the bifurcation structure of the inversion to be investigated without need to estimate this parameter, and demonstrates the expected sensitivity of the bifurcation structure to the underlying surface. The similarity of these results to the vdW17 model is remarkable, considering how highly idealized the vdW17 model is. This fact provides useful guidance for improving the representation of SBL processes in operational weather and climate models and provides a valuable framework for future observational studies of the SBL.

*Acknowledgments.* The Royal Dutch Meteorological Institute (KMNI) provided tower data from the Cabauw Experimental Site for Atmospheric Research (CSESAR) which can be downloaded here: https://ruisdael-observatory.nl/cesar/. Data from the Dome C observatory at the Concordia station in Antarctica are provided through a collaboration with the French Polar Institute Paul-Émile Victor (IPEV) and the Italian National Research Program for Antarctica (PNRA). Data are available through the Concordia Station website: http://www.concordiastation.aq/home-1/. In particular we thank Etienne Vignon for providing additional data and lending his insights into this topic. Hamburg data are provided from the Wettermast, Hamburg, of the Meteorological Institute of the University of Hamburg by Felix Ament and Ingo Lange through Carsten Abraham. Martin Kohler and the Institute for Meteorology and Climate Research of the Karlsruhe Institute of Technology (KIT) generously provided Karlsruhe data. The Los Alamos National Laboratory (LANL)

provided data from the Environmental Monitoring Plan (EMP) which can be downloaded here: https://weathermachine.lanl.gov/TA6.asp. This work would not be possible without the careful collection, maintenance, and accessibility of these datasets generously provided at no cost. The authors thank Carsten Abraham, Hansi Singh, Knut von Salzen, and Marek Stastna for helpful comments on this research. As well, we thank Davide Faranda and two anonymous reviewers for their reviews, which greatly improved the manuscript. We would also like to thank Joachim Peinke for originally suggesting the empirical reconstruction approach. We acknowledge the support of the Natural Sciences and Engineering Research Council of Canada (NSERC), RGPIN-2019-04986.

## REFERENCES

Abraham, C., and A. H. Monahan, 2019a: Climatological features of the weakly and very stably stratified nocturnal boundary layers. Part I: State variables containing information about regime occupation. *J. Atmos. Sci.*, **76**, 3455–3484, https://doi.org/10.1175/JAS-D-18-0261.1.

——, and ——, 2019b: Climatological features of the weakly and very stably stratified nocturnal boundary layers. Part II: Regime occupation and transition statistics and the influence of external drivers. *J. Atmos. Sci.*, **76**, 3485–3504, https://doi.org/10.1175/JAS-D-19-0078.1.

——, and ——, 2019c: Climatological features of the weakly and very stably stratified nocturnal boundary layers. Part III: The structure of meteorological state variables in persistent regime nights and across regime transitions. *J. Atmos. Sci.*, **76**, 3505–3527, https://doi.org/10.1175/JAS-D-18-0274.1.

——, A. M. Holdsworth, and A. H. Monahan, 2019: A prototype stochastic parameterization of regime behaviour in the stably stratified atmospheric boundary layer. *Nonlinear Processes Geophys.*, **26**, 401–427, https://doi.org/10.5194/npg-26-401-2019.

Acevedo, O. C., F. D. Costa, R. Maroneze, A. D. Carvalho, F. S. Puhales, and P. E. S. Oliveira, 2021: External controls on the transition between stable boundary-layer turbulence regimes. *Quart. J. Roy. Meteor. Soc.*, **147**, 2335–2351, https://doi.org/10.1002/qj.4027.

Baas, P., B. J. H. van de Wiel, E. van Meijgaard, E. Vignon, C. Genthon, S. J. A. van der Linden, and S. R. de Roode, 2019: Transitions in the wintertime near-surface temperature inversion at Dome C, Antarctica. *Quart. J. Roy. Meteor. Soc.*, **145**, 930–946, https://doi.org/10.1002/qj.3450.

Barthlott, C., N. Kalthoff, and F. Fiedler, 2003: Influence of high-frequency radiation on turbulence measurements on a 200 m tower. *Meteor. Z.*, **12**, 67–71, https://doi.org/10.1127/0941-2948/2003/0012-0067.

Bosveld, F. C., P. Baas, A. C. M. Beljaars, A. A. M. Holtslag, J. V.-G. de Arellano, and B. J. H. van de Wiel, 2020: Fifty years of atmospheric boundary-layer research at Cabauw serving weather, air quality and climate. *Bound.-Layer Meteor.*, **177**, 583–612, https://doi.org/10.1007/s10546-020-00541-w.

Bowen, B. M., J. A. Baars, and G. L. Stone, 2000: Nocturnal wind direction shear and its potential impact on pollutant transport. *J. Appl. Meteor.*, **39**, 437–445, https://doi.org/10.1175/1520-0450(2000)039<0437:NWDSAI>2.0.CO;2.

Boyko, V., S. Krumscheid, and N. Vercauteren, 2021: Statistical learning of nonlinear stochastic differential equations from non-stationary time series using variational clustering. arXiv, 2102.12395, http://arxiv.org/abs/2102.12395.

Bruggeman, D. A., 2017: Los Alamos climatology 2016 update. LANL Tech. Rep. LA-UR-17-21060, 93 pp., https://doi.org/10.2172/1343690.

Brümmer, B., I. Lange, and H. Konow, 2012: Atmospheric boundary layer measurements at the 280 m high Hamburg weather mast 1995–2011: Mean annual and diurnal cycles. *Meteor. Z.*, **21**, 319–335, https://doi.org/10.1127/0941-2948/2012/0338.

Derbyshire, S. H., 1999: Boundary-layer decoupling over cold surfaces as a physical boundary-instability. *Bound.-Layer Meteor.*, **90**, 297–325, https://doi.org/10.1023/A:1001710014316.

Dijkstra, H. A., and Coauthors, 2014: Numerical bifurcation methods and their application to fluid dynamics: Analysis beyond simulation. *Commun. Comput. Phys.*, **15**, 1–45, https://doi.org/10.4208/cicp. 240912.180613a.

Faranda, D., B. Dubrulle, and F. M. E. Pons, 2014: Statistical early-warning indicators based on autoregressive moving-average models. *J. Phys.*, **47A**, 252001, https://doi.org/10.1088/1751-8113/47/25/252001.

Friedrich, R., and Coauthors, 2000: Extracting model equations from experimental data. *Phys. Lett.*, **271A**, 217–222, https://doi.org/10.1016/S0375-9601(00)00334-0.

——, J. Peinke, M. Sahimi, and M. R. R. Tabar, 2011: Approaching complexity by stochastic methods: From biological systems to turbulence. *Phys. Rep.*, **506**, 87–162, https://doi.org/10.1016/j.physrep.2011.05.003.

García, C. A., A. Otero, P. Félix, J. Presedo, and D. G. Márquez, 2017: Nonparametric estimation of stochastic differential equations with sparse Gaussian processes. *Phys. Rev. E*, **96**, 022104, https://doi.org/10.1103/PhysRevE.96.022104.

Gardiner, C., 1990: *Handbook of Stochastic Methods: For Physics, Chemistry and the Natural Sciences*. Lecture Notes in Mathematics, Springer, 410 pp.

Genthon, C., M. S. Town, D. Six, V. Favier, S. Argentini, and A. Pellegrini, 2010: Meteorological atmospheric boundary layer measurements and ECMWF analyses during summer at Dome C, Antarctica. *J. Geophys. Res.*, **115**, D05104, https://doi.org/10.1029/2009JD012741.

——, D. Six, H. Gallée, P. Grigioni, and A. Pellegrini, 2013: Two years of atmospheric boundary layer observations on a 45-m tower at Dome C on the Antarctic Plateau. *J. Geophys. Res. Atmos.*, **118**, 3218–3232, https://doi.org/10.1002/jgrd.50128.

——, D. E. Veron, E. Vignon, D. Six, J.-L. Dufresne, J.-B. Madeleine, E. Sultan, and F. Forget, 2021: Ten years of temperature and wind observation on a 45-m tower at Dome C, east Antarctic Plateau. *Earth Syst. Sci. Data*, **13**, 5731–5746, https://doi.org/10.5194/essd-13-5731-2021.

Gryning, S.-E., R. Floors, A. Peña, E. Batchvarova, and B. Brümmer, 2016: Weibull wind-speed distribution parameters derived from a combination of wind-lidar and tall-mast measurements over land, coastal and marine sites. *Bound.-Layer Meteor.*, **159**, 329–348, https://doi.org/10.1007/s10546-015-0113-x.

Holdsworth, A. M., and A. H. Monahan, 2019: Turbulent collapse and recovery in the stable boundary layer using an idealized model of pressure-driven flow with a surface energy budget. *J. Atmos. Sci.*, **76**, 1307–1327, https://doi.org/10.1175/JAS-D-18-0312.1.

——, T. Rees, and A. H. Monahan, 2016: Parameterization sensitivity and instability characteristics of the maximum sustainable heat flux framework for predicting turbulent collapse.

*J. Atmos. Sci.*, **73**, 3527–3540, https://doi.org/10.1175/JAS-D-16-0057.1.

Holtslag, A. A. M., and Coauthors, 2013: Stable atmospheric boundary layers and diurnal cycles: Challenges for weather and climate models. *Bull. Amer. Meteor. Soc.*, **94**, 1691–1706, https://doi.org/10.1175/BAMS-D-11-00187.1.

Kaiser, A., D. Faranda, S. Krumscheid, D. Belušić, and N. Vercauteren, 2020: Detecting regime transitions of the nocturnal and polar near-surface temperature inversion. *J. Atmos. Sci.*, **77**, 2921–2940, https://doi.org/10.1175/JAS-D-19-0287.1.

Kalthoff, N., and B. Vogel, 1992: Counter-current and channelling effect under stable stratification in the area of Karlsruhe. *Theor. Appl. Climatol.*, **45**, 113–126, https://doi.org/10.1007/BF00866400.

Kohler, M., J. Metzger, and N. Kalthoff, 2018: Trends in temperature and wind speed from 40 years of observations at a 200-m high meteorological tower in southwest Germany. *Int. J. Climatol.*, **38**, 23–34, https://doi.org/10.1002/joc.5157.

Krumscheid, S., M. Pradas, G. A. Pavliotis, and S. Kalliadasis, 2015: Data-driven coarse graining in action: Modeling and prediction of complex systems. *Phys. Rev. E*, **92**, 042139, https://doi.org/10.1103/PhysRevE.92.042139.

LeMone, M. A., and Coauthors, 2019: 100 years of progress in boundary layer meteorology. *A Century of Progress in Atmospheric and Related Sciences: Celebrating the American Meteorological Society Centennial*, *Meteor. Monogr.*, No. 59, Amer. Meteor. Soc., https://doi.org/10.1175/AMSMONOGRAPHS-D-18-0013.1.

Mahrt, L., 1998: Stratified atmospheric boundary layers and breakdown of models. *Theor. Comput. Fluid Dyn.*, **11**, 263–279, https://doi.org/10.1007/s001620050093.

——, 2014: Stably stratified atmospheric boundary layers. *Annu. Rev. Fluid Mech.*, **46**, 23–45, https://doi.org/10.1146/annurev-fluid-010313-141354.

Monahan, A. H., 2014: Wind speed probability distribution. *Encyclopedia of Natural Resources: Air*, Vol. 2, 1st ed. Taylor and Francis, 1084–1088, https://doi.org/10.1201/9780203757611.

——, and J. Culina, 2011: Stochastic averaging of idealized climate models. *J. Climate*, **24**, 3068–3088, https://doi.org/10.1175/2011JCLI3641.1.

——, T. Rees, Y. He, and N. McFarlane, 2015: Multiple regimes of wind, stratification, and turbulence in the stable boundary layer. *J. Atmos. Sci.*, **72**, 3178–3198, https://doi.org/10.1175/JAS-D-14-0311.1.

Penland, C., 2003: Noise out of chaos and why it won't go away. *Bull. Amer. Meteor. Soc.*, **84**, 921–926, https://doi.org/10.1175/BAMS-84-7-921.

Petenko, I., S. Argentini, G. Casasanta, C. Genthon, and M. Kallistratova, 2019: Stable surface-based turbulent layer during the polar winter at Dome C, Antarctica: Sodar and in situ observations. *Bound.-Layer Meteor.*, **171**, 101–128, https://doi.org/10.1007/s10546-018-0419-6.

Ramsey, E., 2021: Empirical bifurcation analysis of atmospheric stable boundary layer regime occupation. Ph.D. dissertation, University of Victoria, 89 pp., http://hdl.handle.net/1828/12988.

Rasmussen, C. E., and C. K. I. Williams, 2006: *Gaussian Processes for Machine Learning*. MIT Press, 266 pp.

Scheffer, M., and Coauthors, 2009: Early-warning signals for critical transitions. *Nature*, **461**, 53–59, https://doi.org/10.1038/nature08227.

Siegert, S., R. Friedrich, and J. Peinke, 1998: Analysis of data sets of stochastic systems. *Phys. Lett.*, **243A**, 275–280, https://doi.org/10.1016/S0375-9601(98)00283-7.

Sommerfeld, M., C. Crawford, A. Monahan, and I. Bastigkeit, 2019: Lidar-based characterization of mid-altitude wind conditions for airborne wind energy systems. *Wind Energy*, **22**, 1101–1120, https://doi.org/10.1002/we.2343.

Sun, J., and Coauthors, 2002: Intermittent turbulence associated with a density current passage in the stable boundary layer. *Bound.-Layer Meteor.*, **105**, 199–219, https://doi.org/10.1023/A:1019969131774.

——, and Coauthors, 2004: Atmospheric disturbances that generate intermittent turbulence in nocturnal boundary layers. *Bound.-Layer Meteor.*, **110**, 255–279, https://doi.org/10.1023/A:1026097926169.

——, and Coauthors, 2015: Review of wave-turbulence interactions in the stable atmospheric boundary layer. *Rev. Geophys.*, **53**, 956–993, https://doi.org/10.1002/2015RG000487.

Sura, P., and J. Barsugli, 2002: A note on estimating drift and diffusion parameters from timeseries. *Phys. Lett.*, **305A**, 304–311, https://doi.org/10.1016/S0375-9601(02)01474-3.

Twardowska, K., 1996: Wong-Zakai approximations for stochastic differential equations. *Acta Appl. Math.*, **43**, 317–359, https://doi.org/10.1007/BF00047670.

van der Linden, S. J. A., B. J. H. van de Wiel, I. Petenko, C. C. van Heerwaarden, P. Baas, and H. J. J. Jonker, 2020: A Businger mechanism for intermittent bursting in the stable boundary layer. *J. Atmos. Sci.*, **77**, 3343–3360, https://doi.org/10.1175/JAS-D-19-0309.1.

van de Wiel, B. J. H., A. F. Moene, O. K. Hartogensis, H. A. R. De Bruin, and A. A. M. Holtslag, 2003: Intermittent turbulence in the stable boundary layer over land. Part III: A classification for observations during CASES-99. *J. Atmos. Sci.*, **60**, 2509–2522, https://doi.org/10.1175/1520-0469(2003)060<2509:ITITSB>2.0.CO;2.

——, ——, G. J. Steeneveld, O. K. Hartogensis, and A. A. M. Holtslag, 2007: Predicting the collapse of turbulence in stably stratified boundary layers. *Flow Turbul. Combus.*, **79**, 251–274, https://doi.org/10.1007/s10494-007-9094-2.

——, ——, and H. J. J. Jonker, 2012a: The cessation of continuous turbulence as precursor of the very stable nocturnal boundary layer. *J. Atmos. Sci.*, **69**, 3097–3115, https://doi.org/10.1175/JAS-D-12-064.1.

——, ——, ——, P. Baas, S. Basu, J. M. M. Donda, J. Sun, and A. A. M. Holtslag, 2012b: The minimum wind speed for sustainable turbulence in the nocturnal boundary layer. *J. Atmos. Sci.*, **69**, 3116–3127, https://doi.org/10.1175/JAS-D-12-0107.1.

——, and Coauthors, 2017: Regime transitions in near-surface temperature inversions: A conceptual model. *J. Atmos. Sci.*, **74**, 1057–1073, https://doi.org/10.1175/JAS-D-16-0180.1.

van Hooijdonk, I. G. S., J. M. M. Donda, H. J. H. Clercx, F. C. Bosveld, and B. J. H. van de Wiel, 2015: Shear capacity as prognostic for nocturnal boundary layer regimes. *J. Atmos. Sci.*, **72**, 1518–1532, https://doi.org/10.1175/JAS-D-14-0140.1.

——, A. F. Moene, M. Scheffer, H. J. H. Clercx, and B. J. H. van de Wiel, 2017a: Early warning signals for regime transition in the stable boundary layer: A model study. *Bound.-Layer Meteor.*, **162**, 283–306, https://doi.org/10.1007/s10546-016-0199-9.

——, and Coauthors, 2017b: Near-surface temperature inversion growth rate during the onset of the stable boundary layer. *J. Atmos. Sci.*, **74**, 3433–3449, https://doi.org/10.1175/JAS-D-17-0084.1.

Van Ulden, A. P., and J. Wieringa, 1996: Atmospheric boundary layer research at Cabauw. *Bound.-Layer Meteor.*, **78**, 39–69, https://doi.org/10.1007/BF00122486.

Vignon, E., C. Genthon, H. Barral, C. Amory, G. Picard, H. Gallée, G. Casasanta, and S. Argentini, 2017a: Momentum- and heat-flux parametrization at Dome C, Antarctica: A sensitivity study. *Bound.-Layer Meteor.*, **162**, 341–367, https://doi.org/10.1007/s10546-016-0192-3.

——, and Coauthors, 2017b: Stable boundary-layer regimes at Dome C, Antarctica: Observation and analysis. *Quart. J. Roy. Meteor. Soc.*, **143**, 1241–1253, https://doi.org/10.1002/qj.2998.

Wenzel, A., N. Kalthoff, and V. Horlacher, 1997: On the profiles of wind velocity in the roughness sublayer above a coniferous forest. *Bound.-Layer Meteor.*, **84**, 219–230, https://doi.org/10.1023/A:1000444911103.